CHAPTER IV
RESULTS AND DISCUSSION

4.1 Characterization

4.1.1 FT-IR Spectroscopy

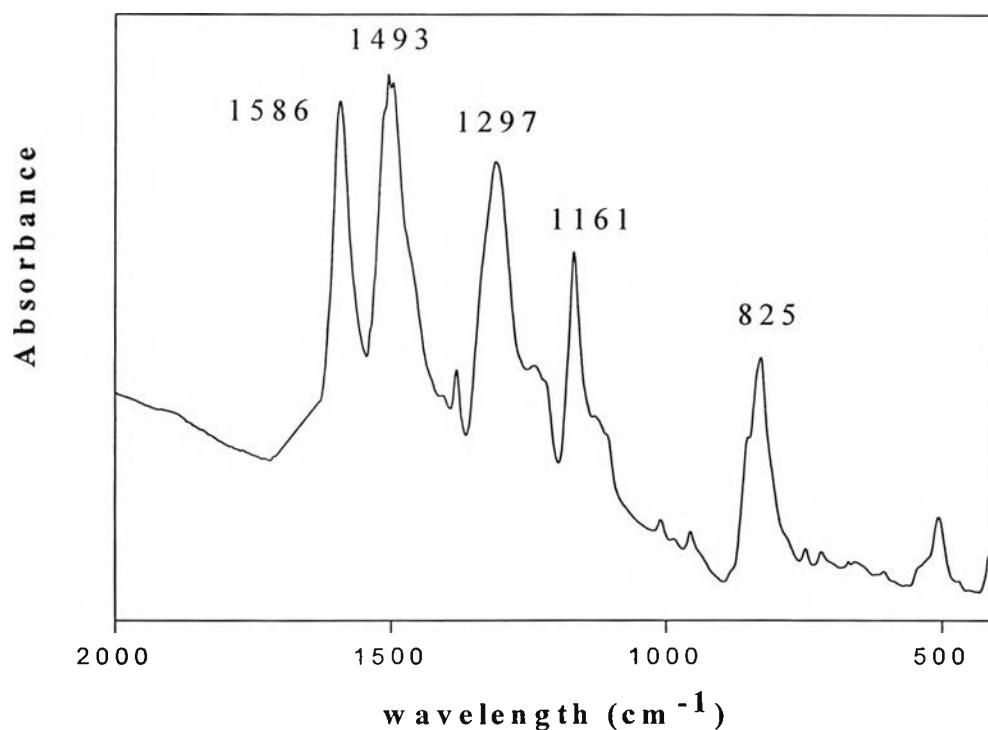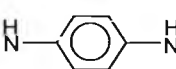The FT-IR spectrum of a synthesized polyaniline (polyaniline

Fig. 4.1 FT-IR spectrum of the synthesized polyaniline emeraldine base.

The spectrum shows five important FT-IR characteristic peaks. Each of the peak position identifies specific characteristic of Polyaniline EB, which can be

related to the chemical bonds. The peak locations and interpretations are tabulated in Table 4.1.

Table 4.1   The characteristic FT-IR peaks of Polyaniline Emeraldine Base (Zeng *et al.* 1998)

Wavelegth (cm^{-1})	Functional Group	
1586	Stretching vibration of N-quinoid ring	
1493	Stretching vibration of N-benzenoid ring	
1297	Stretching vibration of C-N	
1161	Vibration mode of quinoid ring	
825	C-H bending vibration of para-couple benzene ring	

The absorption peaks at 1586 cm^{-1} and 1493 cm^{-1} represent the stretching vibrations of the quinoid ring and the benzenoid ring, respectively (Zeng et al. 1998). This indicates that the synthesized polyaniline was composed of two parts which are the characteristic feature of a polyaniline emeraldine base. The absorption at 1161 cm^{-1} indicates an electronic band which is associated with electrical conductivity of polyaniline (Narayana *et al.* 1994). The absorption at 825 cm^{-1} indicates the type of substituted benzene in polyaniline. Our results are consistent with those of Zeng *et al.* (1998).

The FT-IR spectra of the HCl, CSA and ESA doped polyaniline at various doping ratios (C_a/C_p and N_a/N_p) are shown in Figure 4.2, 4.3 and 4.4, respectively.
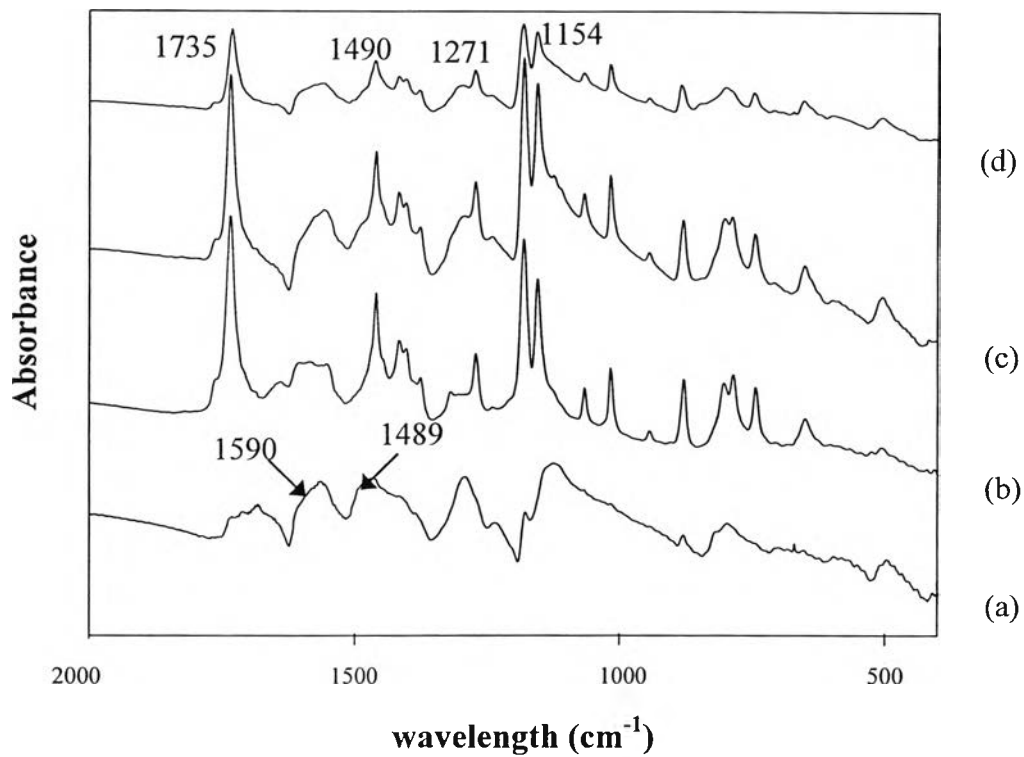
Fig 4.2 FT-IR spectra of HCl-doped polyaniline at various doping ratios: (a) $C_a/C_p = 1$, $N_a/N_p = 9.90$; (b) $C_a/C_p = 10$, $N_a/N_p = 99.3$; (c) $C_a/C_p = 50$, $N_a/N_p = 496$; and (d) $C_a/C_p = 500$, $N_a/N_p = 4963$.
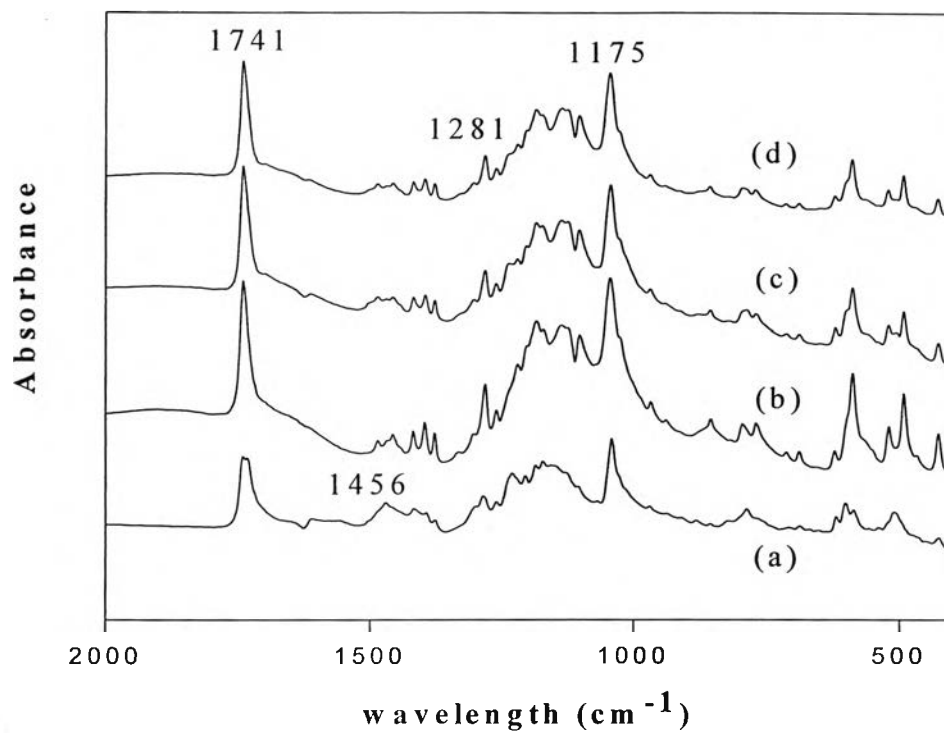
Fig 4.3 FT-IR spectra of CSA-doped polyaniline at various doping ratios: (a) $C_a/C_p= 5$, $N_a/N_p = 7.80$; (b) $C_a/C_p= 50$, $N_a/N_p = 78.1$; (c) $C_a/C_p= 150$, $N_a/N_p = 234$; and (d) $C_a/C_p= 500$, $N_a/N_p = 781$.
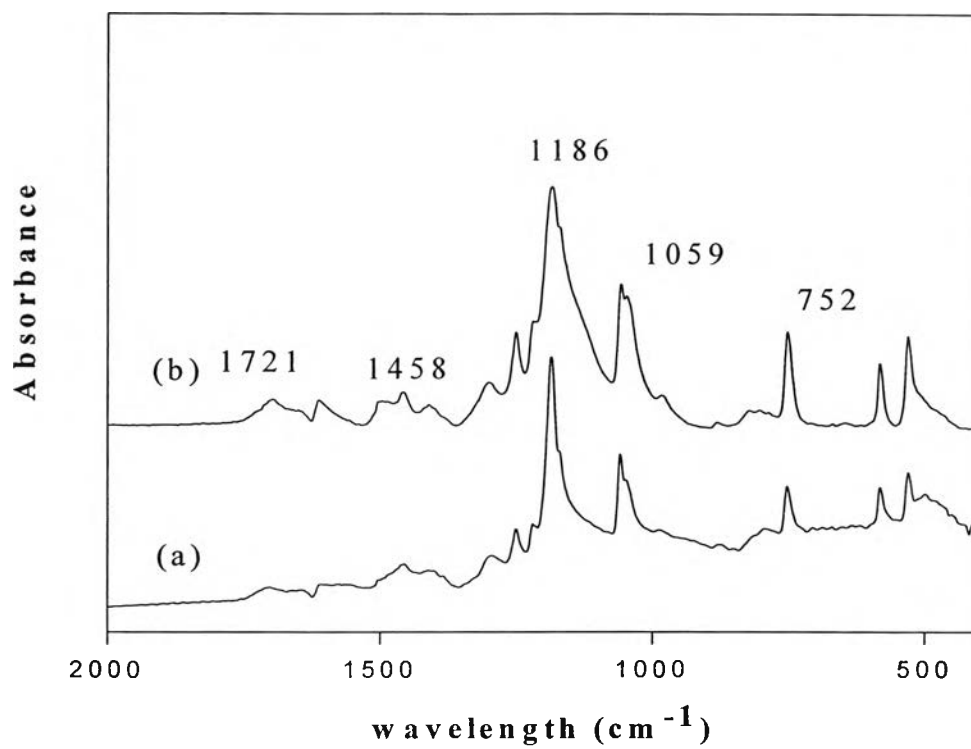
Fig 4.4 FT-IR spectra of ESA-doped polyaniline at various doping ratios: (a) $C_a/C_p = 1$, $N_a/N_p = 3.30$; and (b) $C_a/C_p = 10$, $N_a/N_p = 32.9$.

From FT-IR spectra of the undoped and doped polyaniline films, the observed peaks are summarized in Table 4.2.

Table 4.2 The summarized FT-IR peaks of undoped and doped polyaniline films

Functional group	Wavelength (cm^{-1})				References
	Undoped	HCl	CSA	ESA	
Stretching C=O group of remaining NMP solvent	-	1735	1741	1721	Milton *et al.* 1993
Stretching C=O group of camphorsulfonic acid	-	-	1741	-	Vikki *et al.* 1996
Stretching vibration of N-quinoid ring	1590	-	-	-	Zeng *et al.* 1998
Stretching vibration of N-bezinoid ring	1493	1459	1456	1458	Zeng *et al.* 1998
Aromatic C-N stretching vibration	1297	1271	1281	-	Zeng *et al.* 1998
Sulfonic acid salt group (peak 1)	-	-	1175	1186	The Aldrich Library of FT-IR spectra
Aromatic hydrogen in-plane blending	1161	1154	-	-	Chan *et al.* 1994
Sulfonic acid salt group (peak 2)	-	-	-	1059	The Aldrich Library of FT-IR spectra

The results show that the absorption peaks at 1493 cm^{-1} and 1297 cm^{-1} representing stretching vibration of N-benzenoid ring and aromatic C-N stretching vibration, respectively were found in both the undoped and the three types of doped polyaniline. While the absorption peak at 1590 cm^{-1} representing stretching vibration of N-quinoid ring was observed in only the undoped polyaniline. This indicates that when the undoped polyaniline was doped by acid dopant, the absorption peak at 1590 cm^{-1} disappeared. This was because the structure of the undoped polyaniline consisting more quinoid ring units was converted to the doped polyaniline (polyaniline emeraldine salt) consisting of more benzenoid ring units. All of the doped polyanilines showed a new peak at around 1700 cm^{-1} which identifies the carbonyl group from remaining NMP solvent. For CSA doped polyaniline, this peak also identifies the carbonyl group of camphorsulfonic acid. The absorption peaks at 1175 and 1059 cm^{-1} were found in FT-IR spectra of CSA and ESA–doped polyaniline. These two peaks represent the sulfonic acid salt group generated from the sulfonic acids.

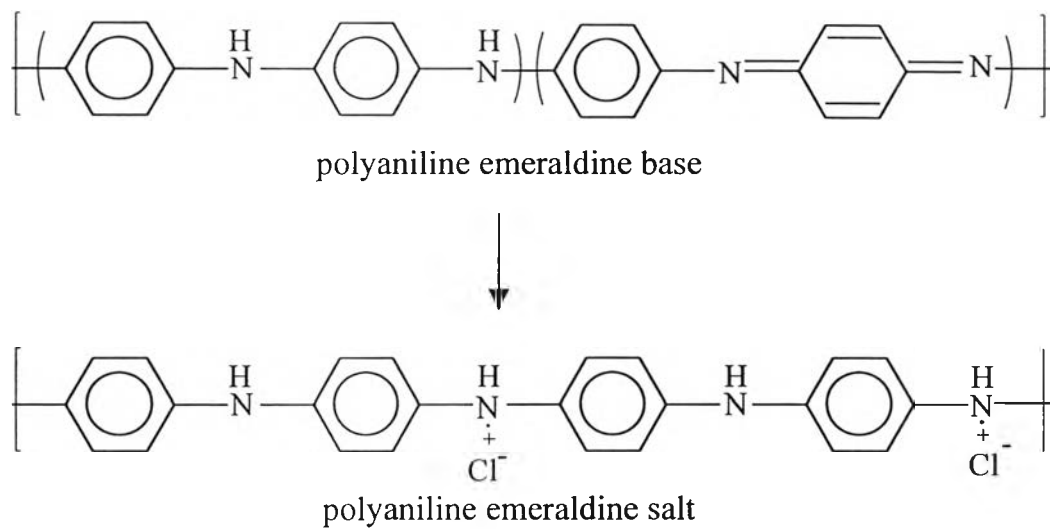The change in chemical structure between Polyaniline EB and Polyaniline ES is chemically depicted in Figure 4.5.

polyaniline emeraldine base

polyaniline emeraldine salt

Fig. 4.5 The change of chemical structure between the polyaniline emeraldine base and the polyaniline emeraldine salt in case of HCl doped polyaniline.

4.1.2 UV-Visible Spectroscopy

The optical properties of conductive polymer play an important role in indicating changes in molecular conformation that affect the electrical properties of a conductive polymer. Figure 4.6 shows an UV-Visible spectrum of synthesized polyaniline EB in NMP solvent.
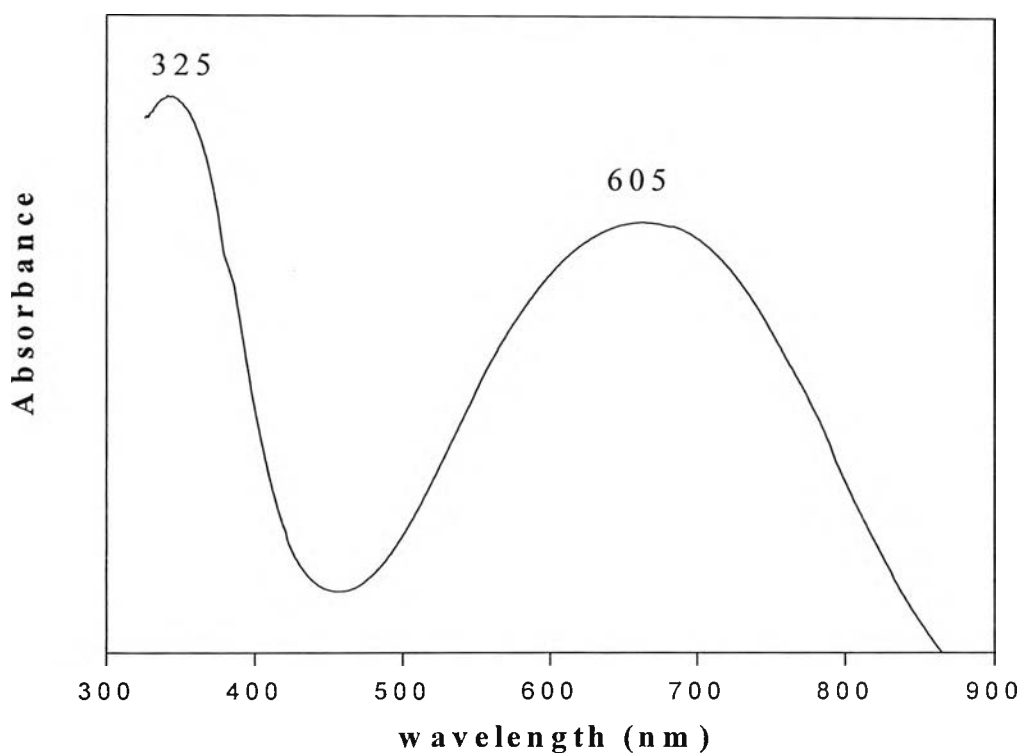

Fig. 4.6 UV-Visible spectrum of synthesized polyaniline emeraldine base in NMP solvent.

The absorption peak at 325 nm indicates the π-π^* transition electrons of the benzene ring delocalized onto nitrogen atoms of the amine in the benzenoid segments. The absorption peak at 605 nm indicates the excitation from the highest occupied molecular orbital (HOMO π_b) of the benzenoid ring to the lowest unoccupied molecular orbital (LUMO π_q) of the localized quinoid segments (Huang *et al.* 1993). The two absorption peaks are observed and identical to those reported by Laakso *et al.* (1994).

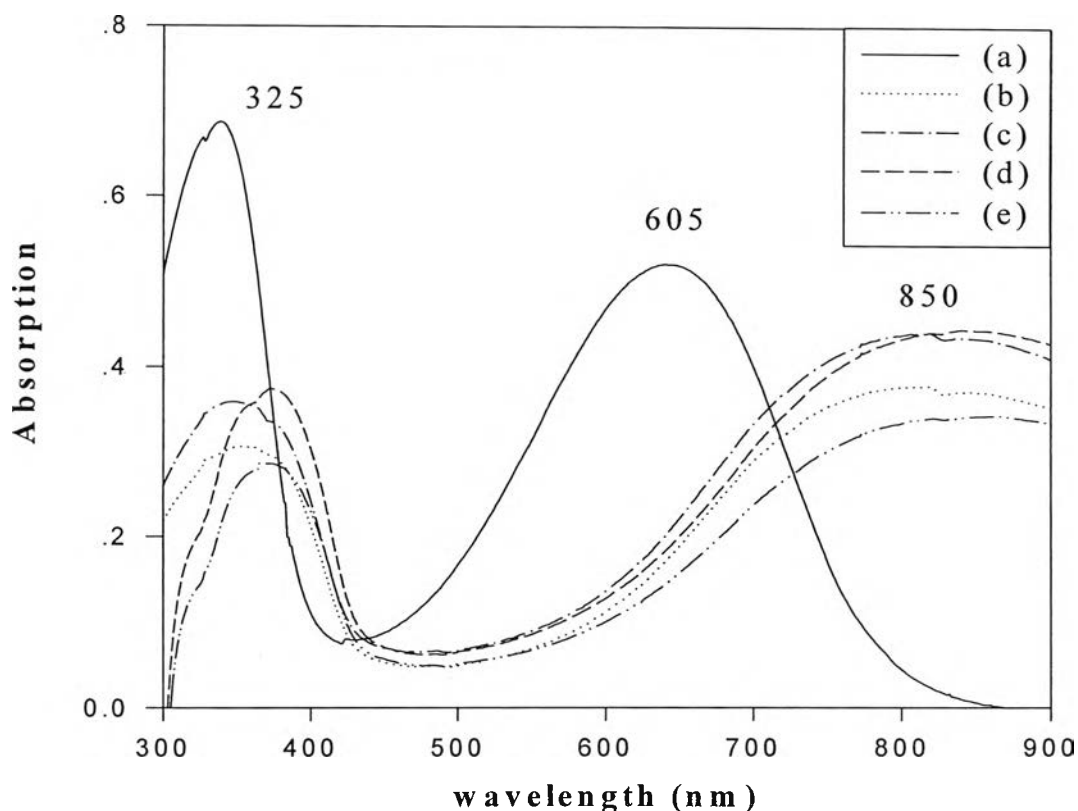The UV-Visible spectra of HCl–doped polyaniline solution at various doping ratios are shown in Figure 4.7.

Fig. 4.7 UV-Visible spectra of HCl-doped polyaniline solution in NMP solvent at various doping ratio: (a) $C_a/C_p = 1$, $N_a/N_p = 9.90$; (b) $C_a/C_p = 5$, $N_a/N_p = 49.6$; (c) $C_a/C_p = 10$, $N_a/N_p = 99.3$; (d) $C_a/C_p = 50$, $N_a/N_p = 496$; and (e) $C_a/C_p = 100$, $N_a/N_p = 993$.

It could be seen that, at the lowest doping ratio ($C_a/C_p = 1$, $N_a/N_p = 9.90$), the two absorption peaks present in Polyaniline EB can still be observed. This indicates that there was no change in the molecular structure at this doping ratio. As the doping ratio increases, starting from $C_a/C_p = 5$, $N_a/N_p = 49.6$, the absorption peak at 605 nm representing the vibration of the quinoid ring segment disappeared because all quinoid sites were reacted by protons of hydrochloric acid and converted to Polyaniline ES. The new absorption peaks

at $\sim$ 850 nm can be observed. This new peak identifies the excitation of the polaron state of the doped polyaniline (Wan 1992). The absorption at 850 nm increased with the increase in the doping ratio up to $C_a/C_p = 50$, $N_a/N_p = 496$. Beyond this doping ratio, the absorption decreased as the doping ratio increased. For $C_a/C_p > 50$, $N_a/N_p > 496$, the doped polyaniline solutions were composed of many protons (H^+) and anions (Cl^-) generated from HCl. Because of these two species, they attempted to combine together to form stable molecules. This reduced the capability of protons to react at quinoid sites, thus the reduction of the polyaniline ES absorption peak at 850 nm was observed.

Figure 4.8 and Figure 4.9 show the UV-Visible spectra of CSA-and ESA-doped polyaniline solutions at various doping ratios, respectively.
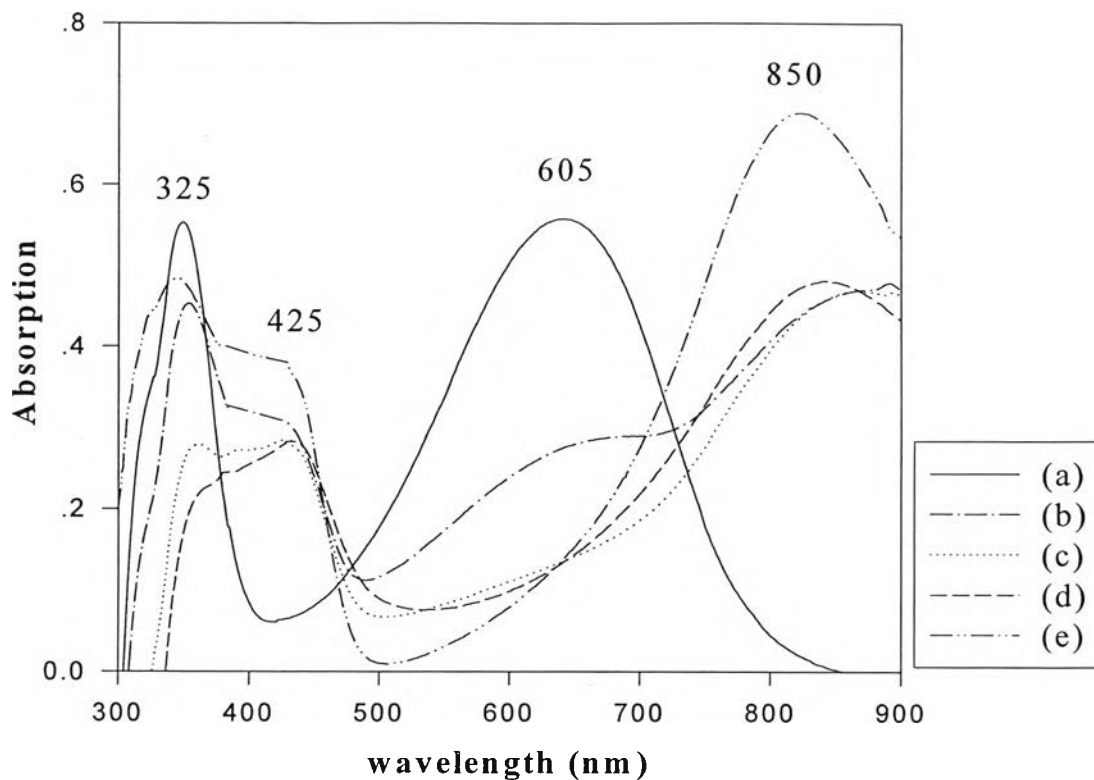
Fig. 4.8 UV-Visible spectra of CSA-doped polyaniline solution in NMP solvent at various doping ratios: (a) $C_a/C_p = 1$, $N_a/N_p = 1.60$; (b) $C_a/C_p = 5$, $N_a/N_p = 7.80$; (c) $C_a/C_p = 10$, $N_a/N_p = 15.6$; (d) $C_a/C_p = 50$, $N_a/N_p = 78.1$; and (e) $C_a/C_p = 150$, $N_a/N_p = 234$.
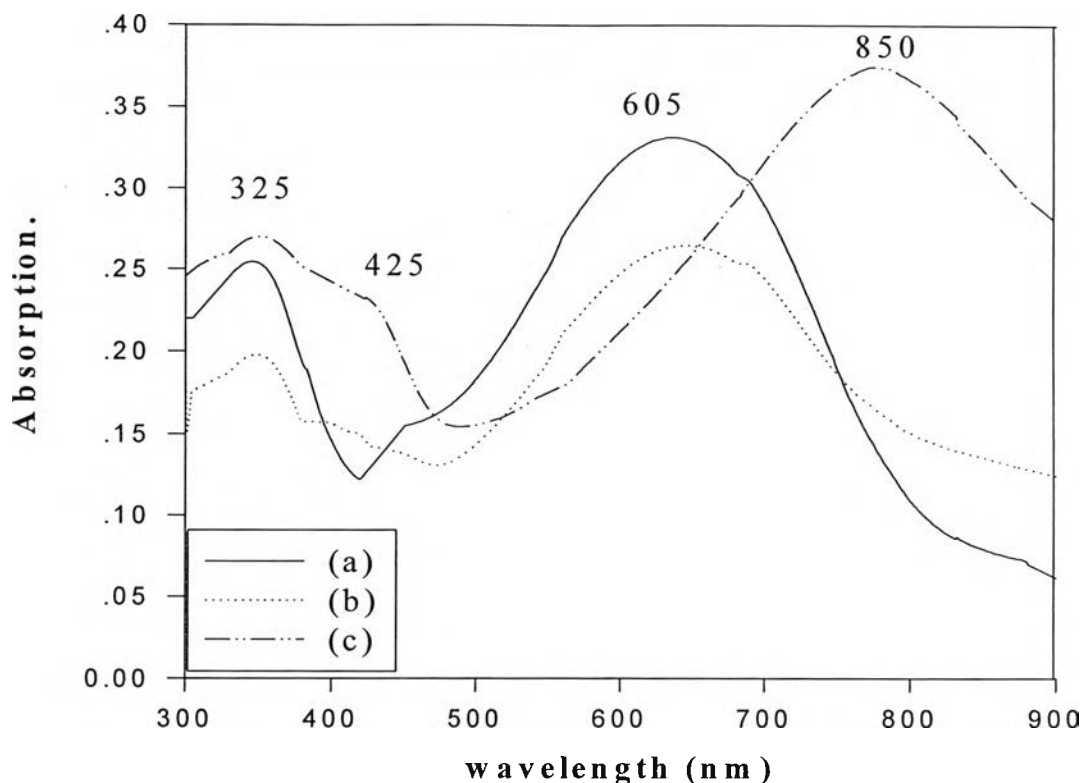
Fig. 4.9 UV-Visible spectra of ESA-doped polyaniline solutions in NMP solvent at various doping ratios: (a) $C_a/C_p = 1$, $N_a/N_p = 3.30$; (b) $C_a/C_p = 5$, $N_a/N_p = 16.5$; and (c) $C_a/C_p = 10$, $N_a/N_p = 32.9$.

It could be observed that the UV-Visible spectra of CSA-doped polyaniline solution at the lowest doping ratio show the same spectrum as that of the polyaniline EB solution. At this doping ratio, the concentration of camphorsulfonic acid as an acid dopant was not high enough to convert an EB (undoped state) to an ES (doped state).

In Figure 4.8, the absorption of the UV-Visible spectra of CSA doped polyaniline at 605 nm decreased when the doping ratio (C_a/C_p) was increased up to 5 whereas the absorptions at 425 and 850 nm representing the polaron state (Sertova *et al.* 1998) increased. But, at the same doping ratio, the UV-Visible spectra of ESA-doped polyaniline solution in Figure 4.9 still show the spectrum of the undoped state. This indicates that at $C_a/C_p = 5$, some part of

EB, as doped by CSA, were converted to ES form while ESA doped polyaniline did not change it form. At higher doping ratios ($C_a/C_p > 5$), the absorption peak at 605 nm for both films completely disappeared. Furthermore, the absorption peaks at 425 and 850 nm were present due to the change in all of the quinoid segments to the bipolaron state and the positive radical of the polaron state in the polyaniline emeraldine salt, respectively (Huang *et al.* 1993).

Therefore, a stronger acid dopant needed a lesser amount of acid dopant for converting a polyaniline in an undoped form to a doped form. The changes in chemical structure from an undoped form to a doped form of these doped polyanilines were identical. The overall results can be summarized in Table 4.3.

Table 4.3 The chemical structures of the undoped state and the doped state of polyanilines (Wan 1992)

State	UV-Visible peak position	Chemical Structure
Undoped State	Polyaniline EB 325 nm: : π-π^* of benenoid segment (a) 605 nm: π-π^* of quinoid segment (b)	
Intermediate State	Polyaniline EB and Polyaniline ES 325 nm: π-π^* of benenoid segment 605 nm: π-π^* of quinoid segment 850 nm: Poly-semiquinone radical cation	
Doped State	Polyaniline ES 325 nm: π-π^* of benenoid segment 425 nm: Bipolaron State 850 nm: Poly-semiquinone radical cation (Polaron State)	

4.1.3 Elemental Analysis (EA)

In the protonation doping process of a polyaniline, the amount of protons from an acid dopant which protonates the nitrogen atoms in the polymer chain can be quantified in terms of doping level. EA was used to determine the amounts of elements; carbon (C), hydrogen (H), nitrogen (N), and sulfer (S) atoms of a doped polyaniline in order to convert to % of H/N or the doping level.

The EA data of % H/N of doped polyaniline films at various doping ratios (C_a/C_p and N_a/N_p) are shown in Table 4.4.

Table 4.4 The EA data of doped polyaniline films

Doped polyaniline	C_a/C_p	N_a/N_p	% H/N
HCl doped polyaniline film	0	0	5.64
	1	9.90	11.3
	10	99.3	13.4
	50	496	14.7
	100	993	13.7
	500	4963	10.4
CSA doped polyaniline films	0	0	5.64
	1	1.60	18.8
	5	7.80	27.6
	10	15.6	28.0
	50	78.1	42.7
	150	234	46.0
	500	781	53.3

Figure 4.10 and Figure 4.11 show the doping levels of HCl and CSA doped polyaniline films from EA measurement as a function of mass and molar doping ratios: C_a/C_p and N_a/N_p.
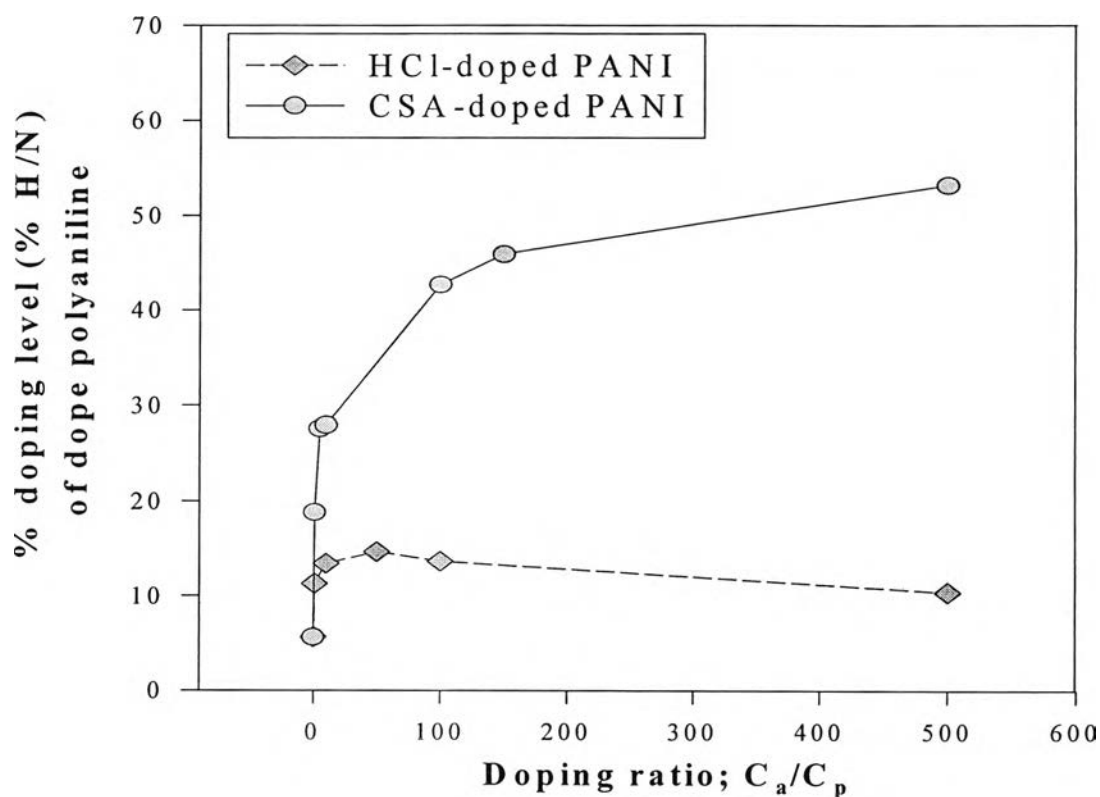

Fig. 4.10 The % doping level of HCl and CSA doped polyaniline films at various doping ratios (C_a/C_p).
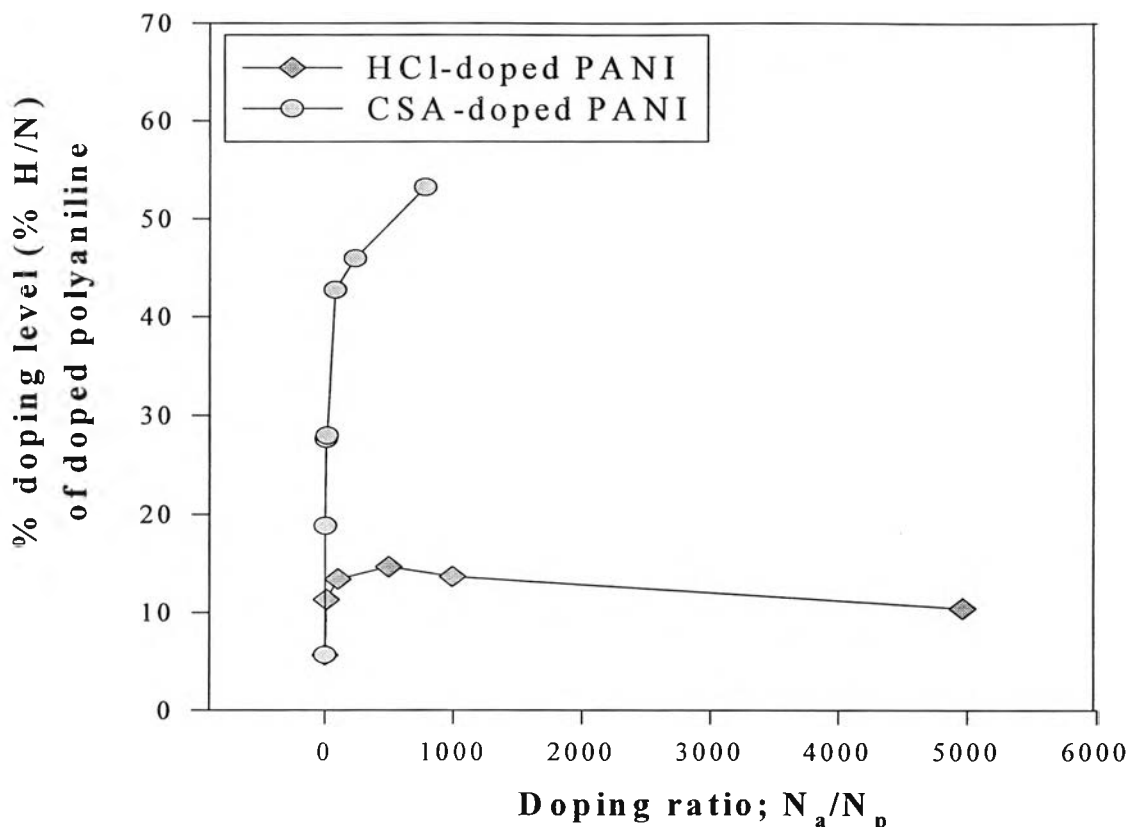
Fig. 4.11 The % doping level of HCl and CSA doped polyaniline films at various doping ratios (N_a/N_p).

Figure 4.11 shows that the doping level of the HCl doped polyaniline at low molar doping ratio increases with the doping ratio. At N_a/N_p equal to 496, the highest doping level was obtained corresponding to the highest protonation. Above N_a/N_p equal to 496, the doping level decreases with increasing doping ratio. In the case of the CSA doped polyaniline, the doping level increases dramatically and monotonically with increasing doping ratio. Due to the film processing and preparation problem, the doping level of the CSA doped polyaniline at high doping ratio could not be studied. At the doping ratio equal to 0, nonzero doping levels were obtained. This was due to the excess amount of the HCl acid obtained from the synthesis.

The doping level of HCl doped polyaniline decreases when $N_a/N_p >$ 496 because the probability of protons to react at the quinoid sites decreased.

In this condition, hydrochloric acid, a strong acid, produced many protons. Because these protons were quite active species, they attempted to combine with anions more than to react with nitrogen atoms at the quinoid rings. This caused a reduction in the doping level.

Comparing the doping levels of the HCl and CSA doped polyanilines, it could be seen that the doping level of CSA-doped polyaniline is higher than the doping level of HCl-doped polyaniline at the same molar doping ratio. This was because the size of the counteranion of camphorsulfonic acid was bigger. This caused the CSA doped polyaniline to have larger free volumes which allowed protons to protonate the polyaniline chains.

4.1.4 X-ray diffractometer (XRD)

XRD technique was used to investigate the order and the degree of crystallinity of the doped polyanilines. The XRD patterns of the HCl, CSA and ESA doped polyaniline films at various doping ratios are shown in Figure 4.12, 4.13 and 4.14, respectively.
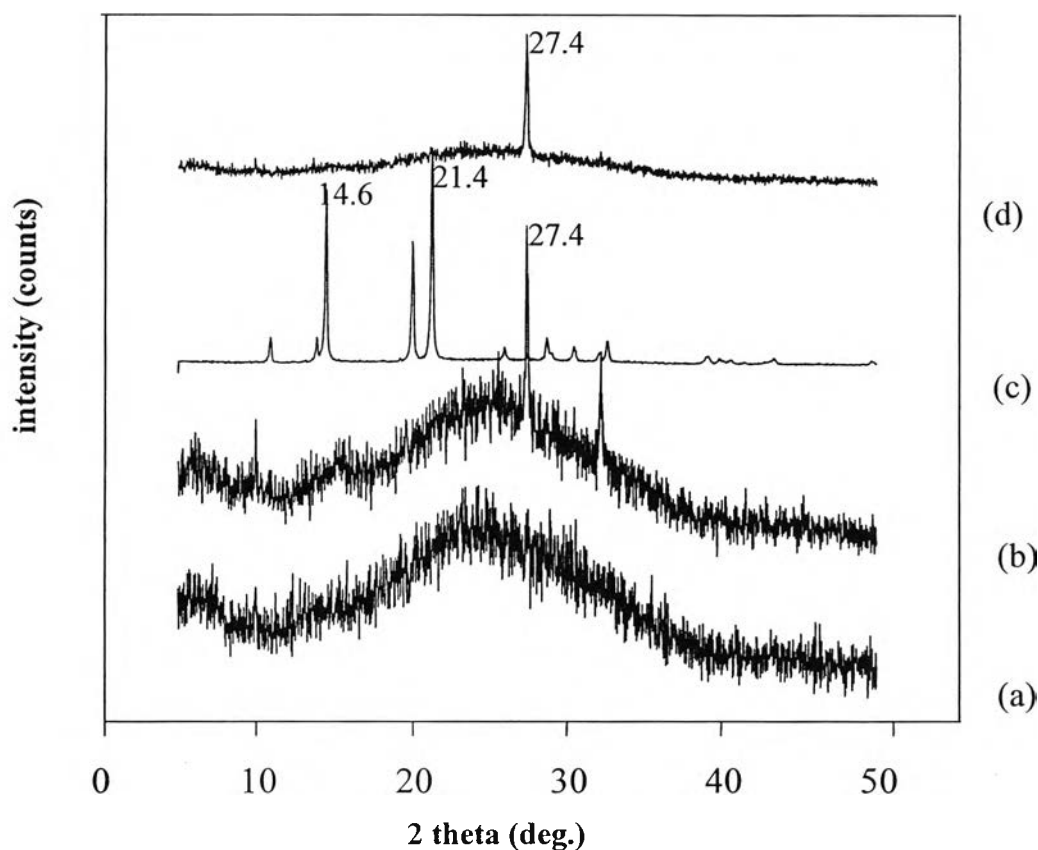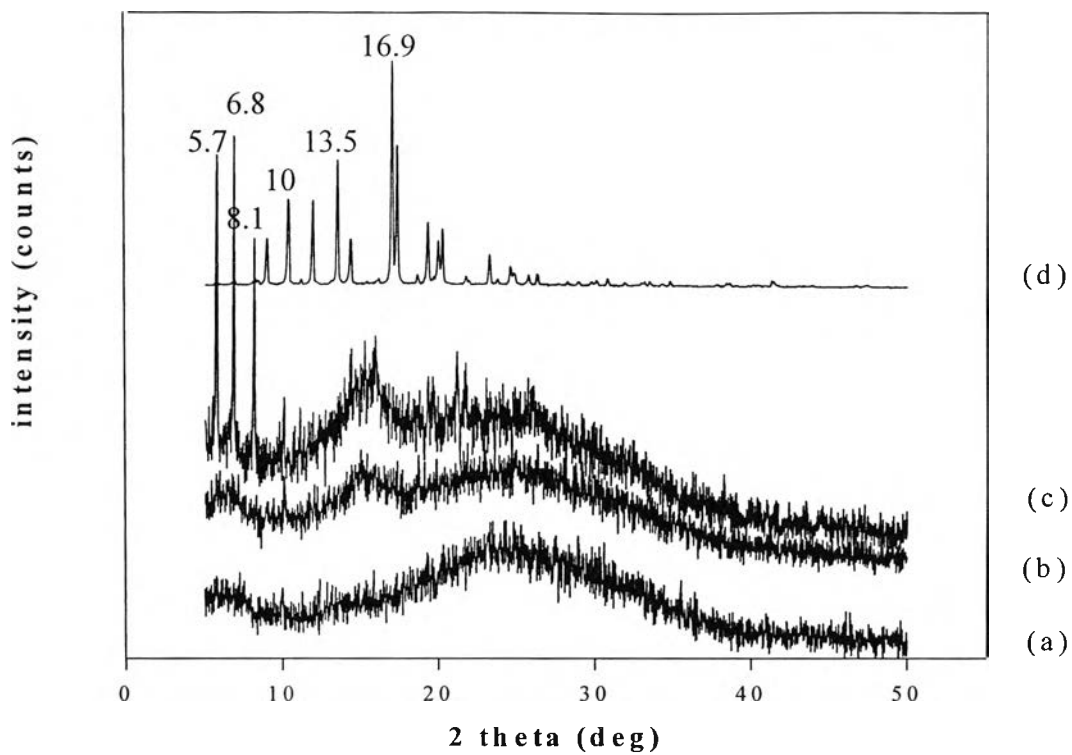

Fig. 4.12 X-ray diffraction patterns of HCl-doped polyaniline films at various doping ratios: (a) $C_a/C_p = 0$, $N_a/N_p = 0$; (b) $C_a/C_p = 1$, $N_a/N_p = 9.90$; (c) $C_a/C_p = 50$, $N_a/N_p = 496$; and (d) $C_a/C_p = 500$, $N_a/N_p = 4963$.

Fig. 4.13 X-ray diffraction patterns of CSA-doped polyaniline films at various doping ratios: (a) $C_a/C_p = 0$, $N_a/N_p = 0$; (b) $C_a/C_p = 1$, $N_a/N_p = 1.60$; (c) $C_a/C_p = 5$, $N_a/N_p = 7.80$; and (d) $C_a/C_p = 10$, $N_a/N_p = 15.6$.
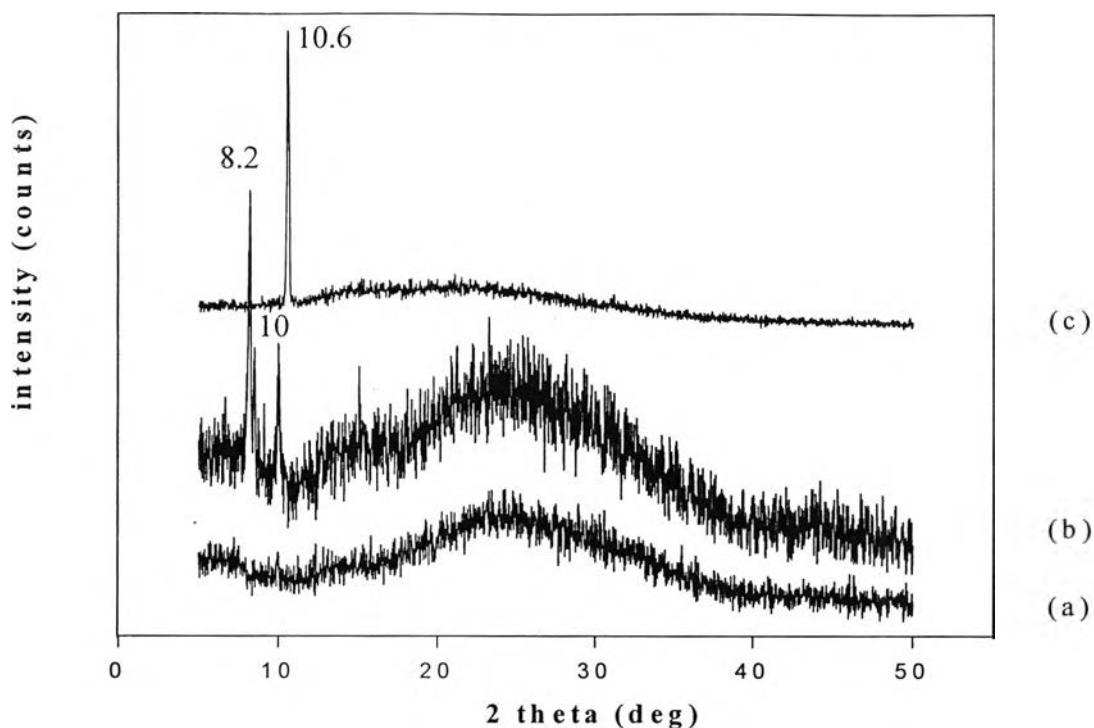
Fig. 4.14 X-ray diffraction patterns of ESA-doped polyaniline films at various doping ratios: (a) $C_a/C_p = 0$, $N_a/N_p = 0$; (b) $C_a/C_p = 1$, $N_a/N_p = 3.30$; and (c) $C_a/C_p = 10$, $N_a/N_p = 32.9$.

The XRD results can be analyzed in term of the Bragg's law: $2d\sin\theta = n\lambda$ (Cempbell *et al.* 1989). The d-value represents the distance between lacttices planes. The theta (θ), n, and λ identify Bragg' s angle, an integer, and wavelength, respectively. From XRD patterns in Figure 4.12-4.14, the values of 2θ and d-value of doped polyanilines are listed in Table 4.5.

Table 4.5 The values of 2theta and d-value of doped polyaniline films

Doped polyaniline	N_a/N_p	2θ (°)	d-value (Å)	Range of d-value (Å)
HCl doped polyaniline films	9.90	27.4	3.30	3.30 - 6.10
	496	14.6	6.10	
		21.4	4.40	
	4963	27.4	3.30	
CSA doped polyaniline films	7.80	5.70	15.5	5.20 – 15.5
		6.80	13.0	
		8.10	10.9	
	15.6	10.0	8.80	
		13.5	6.60	
		16.9	5.20	
ESA doped polyaniline films	3.30	8.20	10.8	8.30 – 10.8
		10.0	8.80	
	32.9	10.6	8.30	

The XRD pattern of the undoped polyaniline film has a broad peak representing as amorphous structure. In the case of the HCl doped polyaniline, the XRD patterns show peaks at 3.30 Å at N_a/N_p equal to 9.90, and peaks at 6.10 and 4.40 Å at N_a/N_p equal to 496. The broad XRD peak and the sharp peak at 3.30 Å were recovered when N_a/N_p is equal to 4963. The XRD pattern of the CSA doped polyaniline shows peaks at 15.5, 13.0, and 10.9 Å at N_a/N_p equal to 7.80 and peaks at 8.80, 6.60, and 5.20 Å at N_a/N_p equal to 15.6. For the ESA doped polyaniline, the peaks were found at 10.8 and 8.80 Å at N_a/N_p equal to 3.30 and a peak at 8.3 Å at N_a/N_p equal to 32.9.

The structures of doped polyaniline related to XRD results are proposed and shown in Table 4.6.

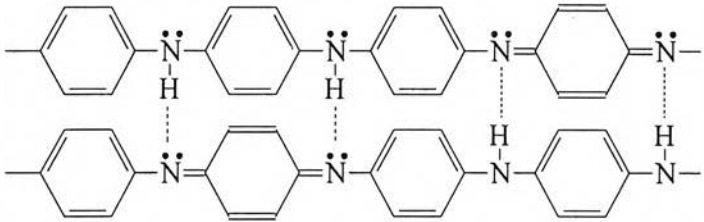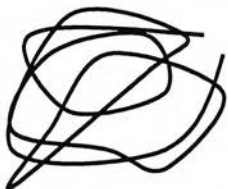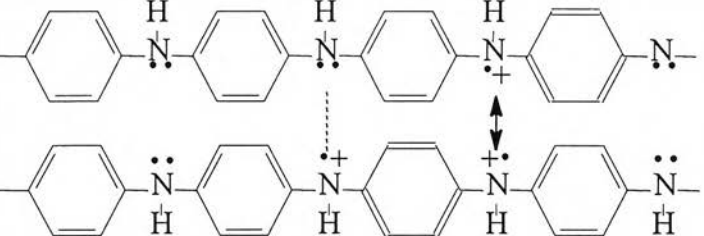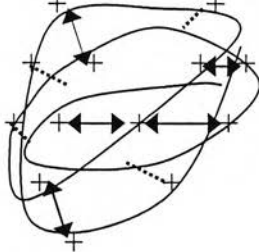**Table 4.6** The proposed structures of doped polyaniline related to XRD results
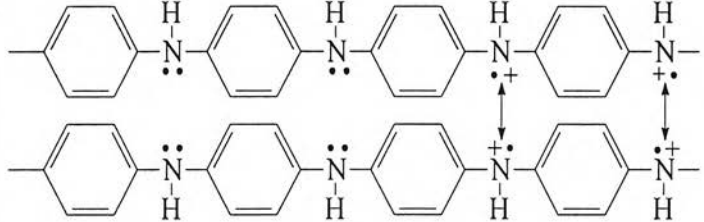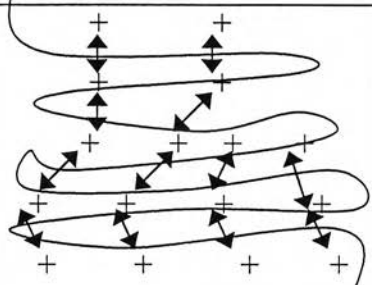
State	Chemical Structure	Proposed Model	XRD result
Undoped			Compact coil (amorphous)
Low doping level			Partially crystalline
High doping level			Expanded chain (more crystalline)

Table 4.6 indicates that a compact coil structure of the polymer chains resulting from the hydrogen bonding between amine and imine positions was observed for the undoped state. Thus, the XRD pattern of the undoped polyaniline reveals the amorphous structure. When polyaniline was protonated by an acid dopant, the protonation at nitrogen positions occurred inducing the positive charges along the chain. Due to the repulsive forces between positive charges along the chain, an expansion of the polyaniline coils structure was observed. This induced the XRD patterns of all doped polyanilines to have some crystalline structures. At a low doping ratio, a partial crystallinity was observed. The large distance between polymer chains with corresponding high d-value occurred because of the lesser repulsive forces between positive charges along the chain. On the contrary, at a high doping ratio, the expanded structure was observed. This resulted in low d-values because the polymer chains could pack closer. But in the case of the HCl doped polyaniline at a high doping ratio, the compact coil structure was recovered. This was due to the favorable interaction between protons and anions causing the reduction in the repulsive forces generated from positive charges along the chain.

Among the d-values of the three types of doped polyaniline, the HCl-doped polyaniline films showed the lowest d-value due to a better packing of polyaniline chains because of a very small size of the counteranion group in the doped polyaniline chains. In the case of the CSA and ESA doped polyaniline films, they had the higher d-values from the looser packing of the polyaniline chains due to bigger sizes of the counteranion groups. From the d-values of each type of doped polyaniline films, it can be inferred that the higher d-values may describe the distance between doped polymer chains. On the contrary, the lower d-values may describe the distance between the dopant molecules and the doped polymer chains.

Luzny *et al.* (2000) reported that the higher d-value at 18 Å can be related to the ordering of dopant molecules between polyaniline chains. On the contrary, the lower d-value at 3.5 Å can be refered to as the distance between two adjacent dopant molecules.

4.2 Electrical Conductivity of Doped Polyaniline Films

4.2.1 Effect of aging

Effect of aging on the electrical conductivity of HCl, CSA and ESA doped polyaniline film at various doping ratios are shown in Figures 4.15, 4.16 and 4.17, respectively.
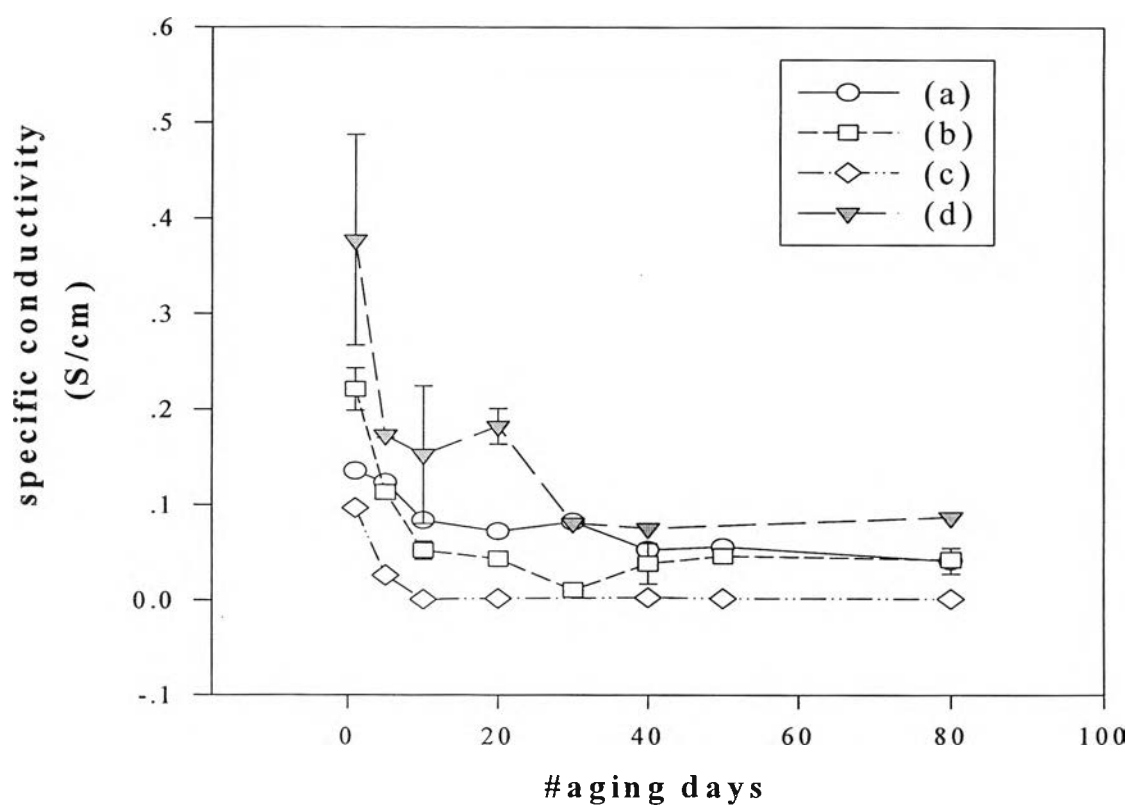

Fig. 4.15 The electrical conductivity (σ) of HCl-doped polyaniline film as a function of time (days) at various doping ratios: (a) $C_a/C_p = 1$, $N_a/N_p = 9.90$; (b) $C_a/C_p = 10$, $N_a/N_p = 99.3$; (c) $C_a/C_p = 50$, $N_a/N_p = 496$; and (d) $C_a/C_p = 500$, $N_a/N_p = 4963$.
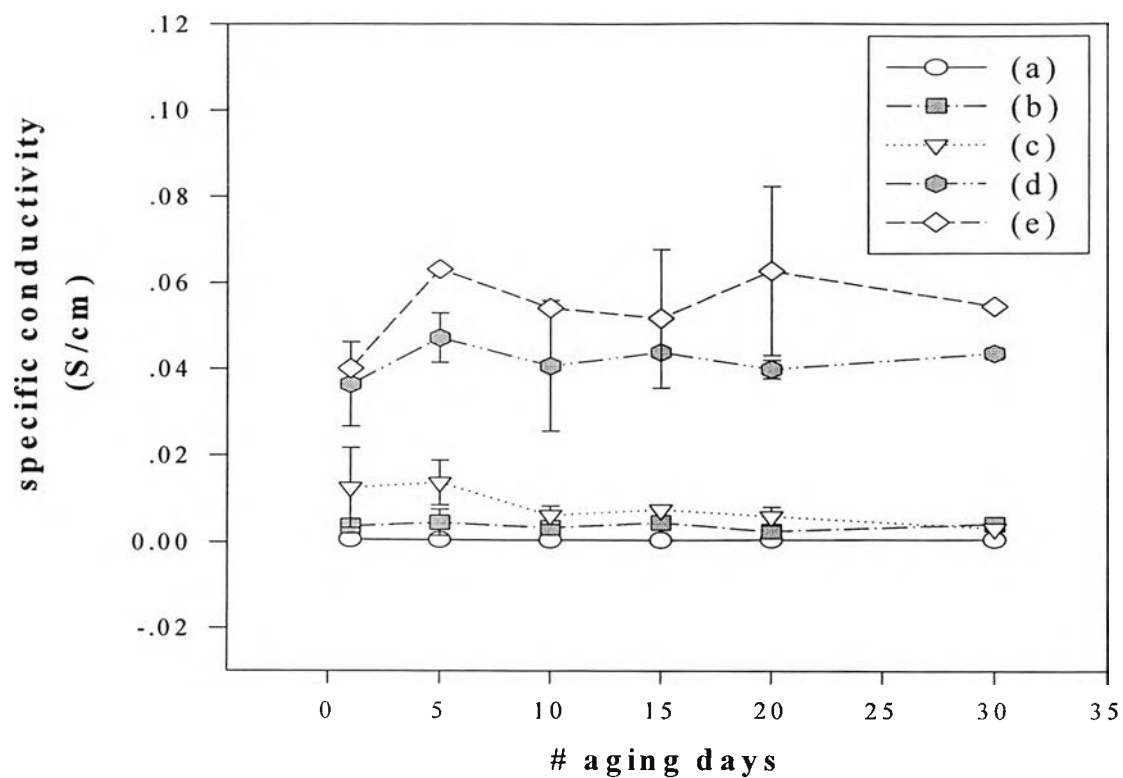
Fig. 4.16 The electrical conductivity (σ) of CSA-doped polyaniline film as a function of time (days) at various doping ratios: (a) $C_a/C_p = 1$, $N_a/N_p = 1.60$; (b) $C_a/C_p = 5$, $N_a/N_p = 7.80$; (c) $C_a/C_p = 10$, $N_a/N_p = 15.6$; (d) $C_a/C_p = 100$, $N_a/N_p = 156$; and (e) $C_a/C_p = 150$, $N_a/N_p = 234$.
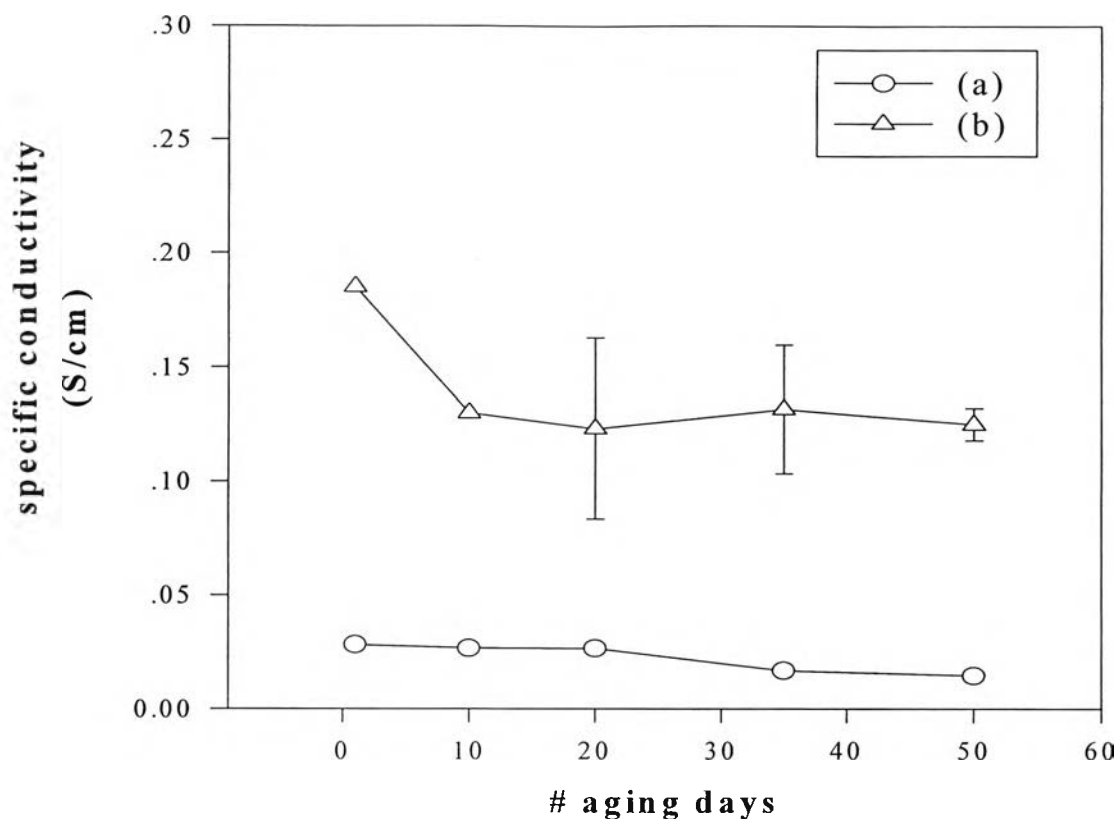
Fig. 4.17 The electrical conductivity (σ) of ESA-doped polyaniline film as a function of time (days) at various doping ratios: (a) $C_a/C_p = 1$, $N_a/N_p = 3.30$; and (b) $C_a/C_p = 10$, $N_a/N_p = 32.9$.

Figure 4.15 indicates that the electrical conductivity of the HCl-doped polyanilines of all doping ratios rapidly decreased during the period of 1 to 20 days. After this period, the equilibrium electrical conductivity was obtained. The highest electrical conductivity was observed at $C_a/C_p = 50$, $N_a/N_p = 496$ corresponding to the highest doping level. In figure 4.16 and 4.17 show a different trend in comparison to the electrical conductivity of the HCl-doped polyaniline films. The electrical conductivity of the CSA and ESA doped polyaniline films at all doping ratio showed no significant change during the first 30 and 50 days, respectively.

Due to the loss of traces of water and/or dopant molecules (MacDiarmid *et. at.* 1989), the electrical conductivity of HCl doped

polyaniline decreased. But in the case of CSA and ESA doped polyaniline, the loss of traces of water and/or dopant molecules did not occur. This may be due to the presence of the bulky counteranion groups, $[(C_{10}H_{15}O)(SO_3^-)]$ and (CH_3CH_2), screening the water molecules from escaping. This phenomenon will be discussed further in section 4.2.3.

4.2.2 Effect of Moisture Content and Humidity

From the results in section 4.2.1, the decrease in the electrical conductivity of the HCl-doped polyaniline film with aging time can be related to the loss of water molecules in films. On the other hand, the electrical conductivity of the CSA-doped polyaniline film shows no dependence. To confirm this relation, the moisture content in film and percentage of humidity identifying the amount of water molecules in the polymer films were varied in order to study their effect on electrical conductivity.

(a) Moisture Effect

Effect of moisture content in film on the electrical conductivity of the HCl and CSA doped polyaniline film is shown in Figure 4.18.
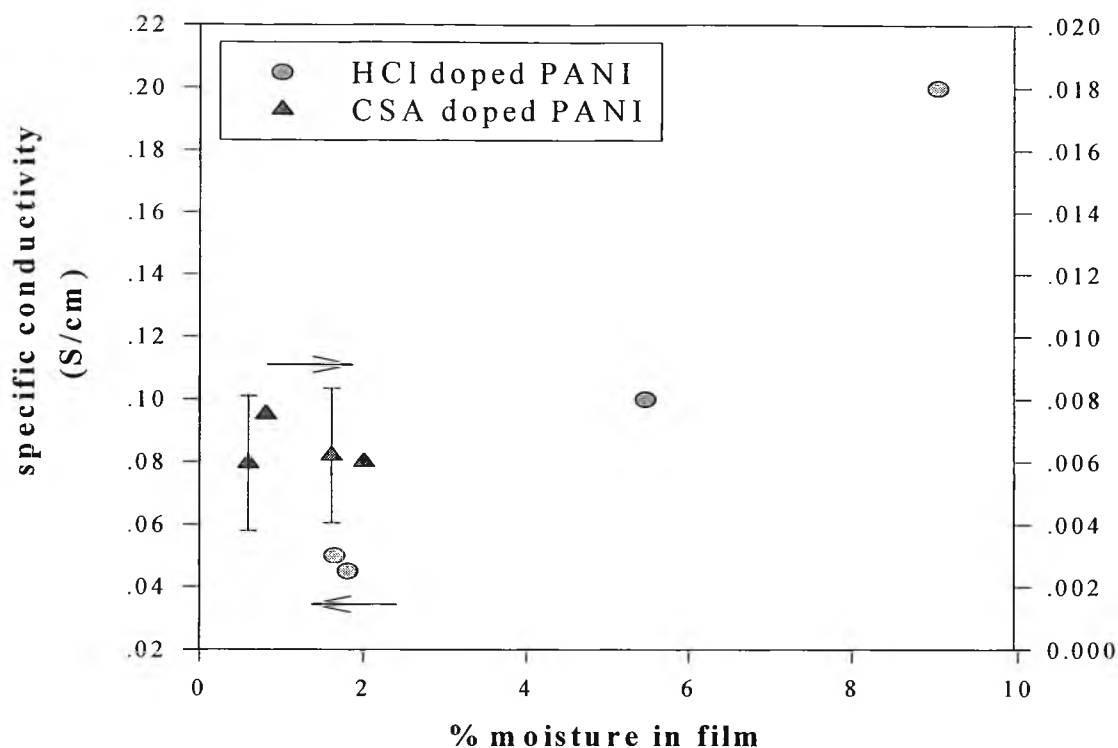
Fig. 4.18 Effect of % moisture in film of the HCl and CSA doped polyaniline films on the electrical conductivity: (a) HCl doped polyaniline film at C_a/C_p = 10, N_a/N_p = 99.3 and % humidity = 65; and (b) CSA doped polyaniline film at C_a/C_p = 10, N_a/N_p = 15.3 and % humidity = 62.

In Figure 4.18, the moisture content in film was measured by the TGA technique. The % humidity of the HCl and CSA doped polyaniline films was controlled at 65 and 62, respectively during the measurements of the electrical conductivity. This graph shows that the electrical conductivity of HCl doped polyaniline films increases with the percentage of moisture. But the electrical conductivity of CSA doped polyaniline film shows only a slight change when moisture content.

(b) Humidity Effect

Effect of humidity on the electrical conductivity of the HCl and CSA doped polyaniline film is shown in Figure 4.19.
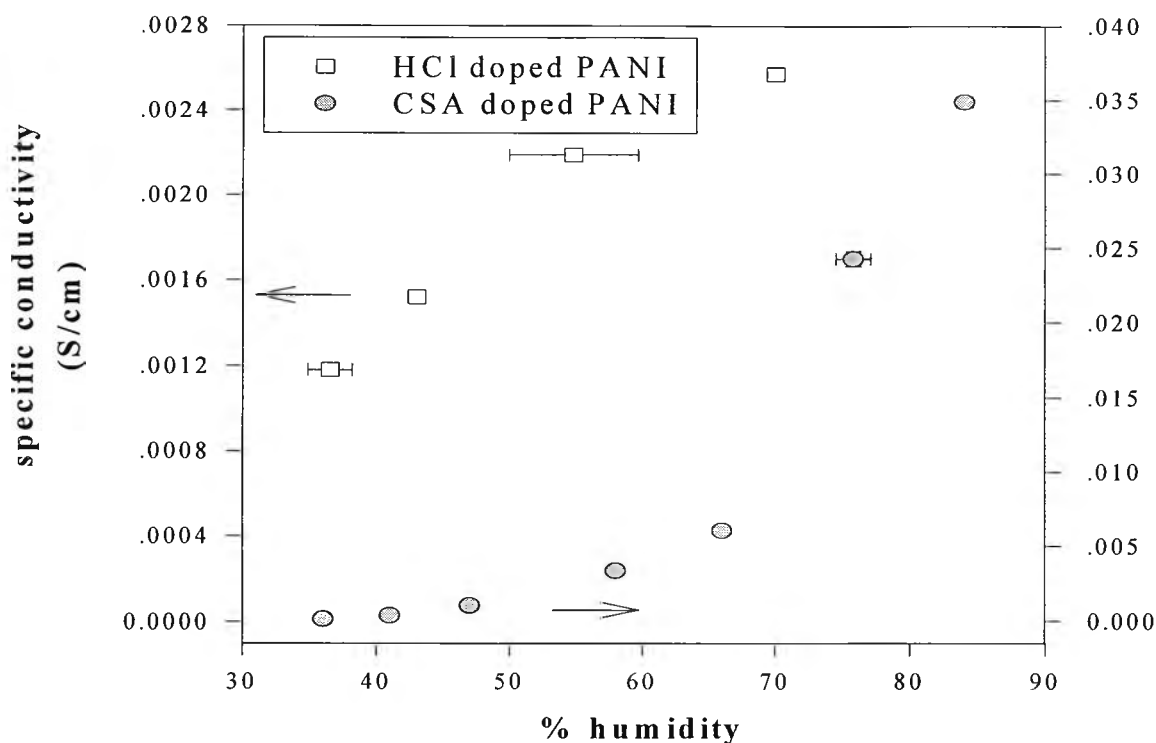

Fig. 4.19 Effect of % humidity of the HCl and CSA dope polyaniline film on the electrical conductivity: (a) HCl doped polyaniline film at $C_a/C_p = 1$, N_a/N_p = 9.90 and % moisture in film < 2; and (b) CSA dope polyaniline film at C_a/C_p = 10, N_a/N_p = 15.3 and % moisture in film < 4.

In Figure 4.19, the starting % moisture in HCl doped polyaniline film was controlled to be less than 2%. This graph shows that the electrical conductivity of HCl doped polyaniline film increased linearly with the percentage of humidity. In case of CSA doped polyaniline film, the starting % moisture in film was controlled at 4%. We found that at low % humidity in range of 30 to 60, the electrical conductivity did not significantly change with % humidity. Beyond that the electrical conductivity rapidly increased with % humidity.

The results in Figure 4.18 and 4.19 can be explained by a conductivity theory (Cowie, 1991). The electrical conductivity is a function of the charge carriers of species "i" (n_i), the charge on each carrier ($\in_i$), and carrier mobilities (μ_i) as described by the relation $\sigma = \Sigma\mu_i n_i \in_i$ (Cowie, 1991). The electrical conductivity of conductive polymer depends on charge mobility on polymer chains. This means that the electrical conductivity increases with the mobility of ion on polymer chains. Figure 4.20 shows the proposed model that explains effect of moisture content and humidity on the electrical conductivity of dope polyaniline.
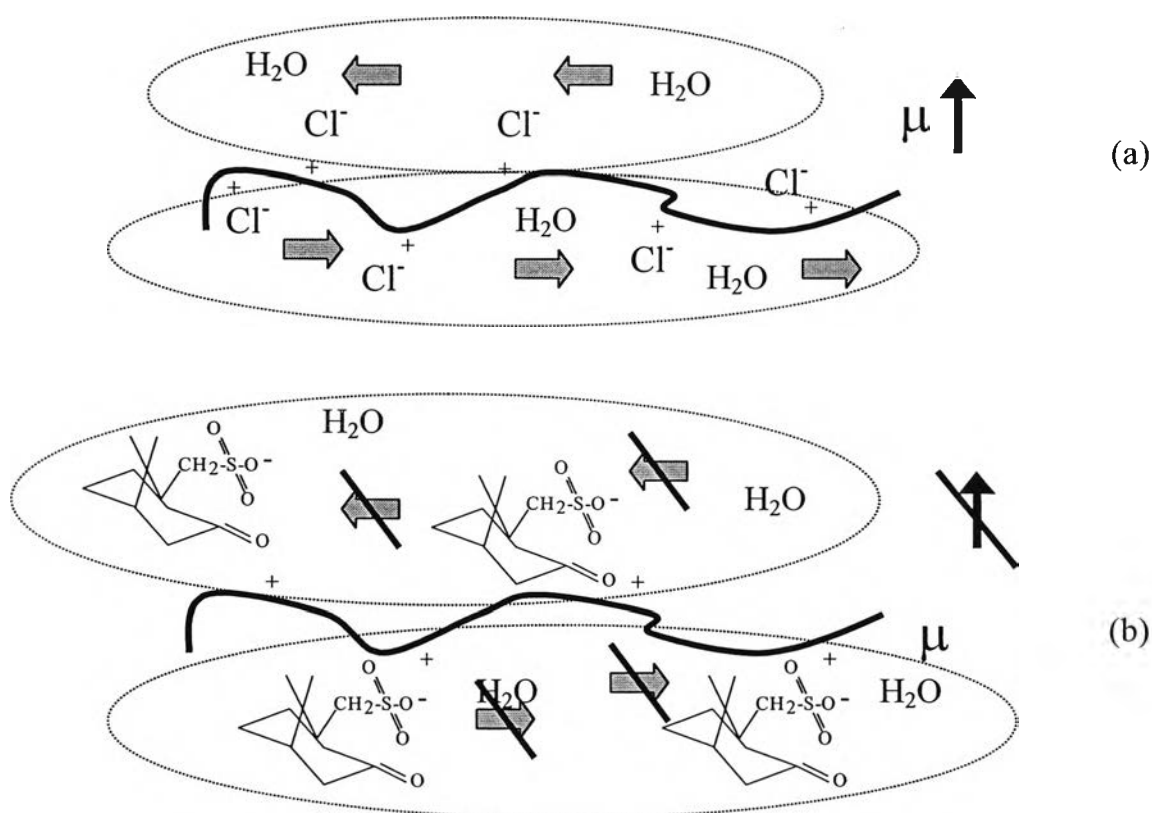

Fig 4.20 The proposed model on the effect of moisture and humidity on the electrical conductivity of doped polyaniline: (a) HCl-doped polyaniline; (b) CSA-doped polyaniline.

From the conductivity theory, the electrical conductivity of the doped polyaniline increased when water molecules inside doped film moved counteranions causing the charge mobility increased (Cowie, 1991). In Figure 4.20, and in case of the HCl-doped polyaniline film, because of the small size of chloride ions acting as a counteranion of the HCl-doped polyaniline, water molecules could move these charge carriers. Therefore the electrical conductivity of HCl-doped polyaniline increased when % moisture and humidity increased. In contrast, the camphorsulfonate ions acting as a counteranion of the CSA-doped polyaniline could not move and be moved by water molecules because of their bigger anion group. This caused the electrical conductivity of the CSA-doped polyaniline did not change. But, at high percentage of humidity, the increase in the electrical conductivity of the CSA-doped polyaniline was observed. It was due to the camphorsulfonate anions could be moved by many amounts of water molecule.

4.2.3 Effect of acid concentration on the electrical conductivity of doped polyaniline film

Effect of acid concentration on the electrical conductivity of HCl, CSA and ESA doped polyaniline films at various doping ratios is shown in Figure 4.21.
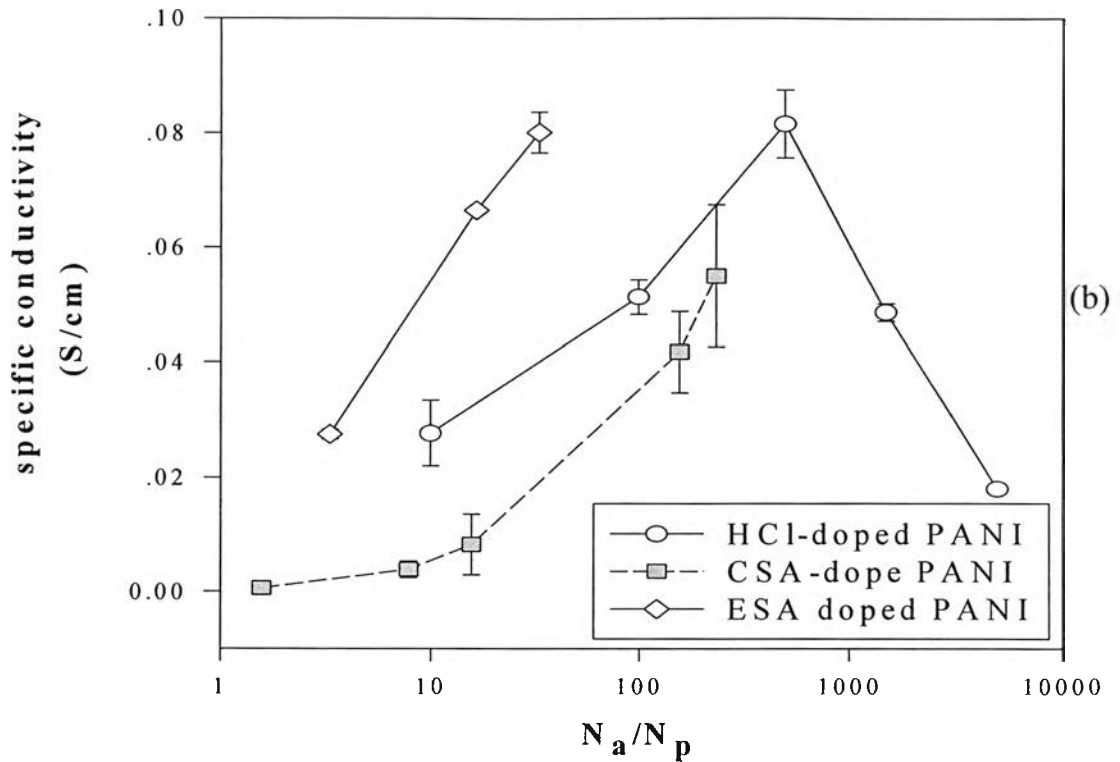

(a)
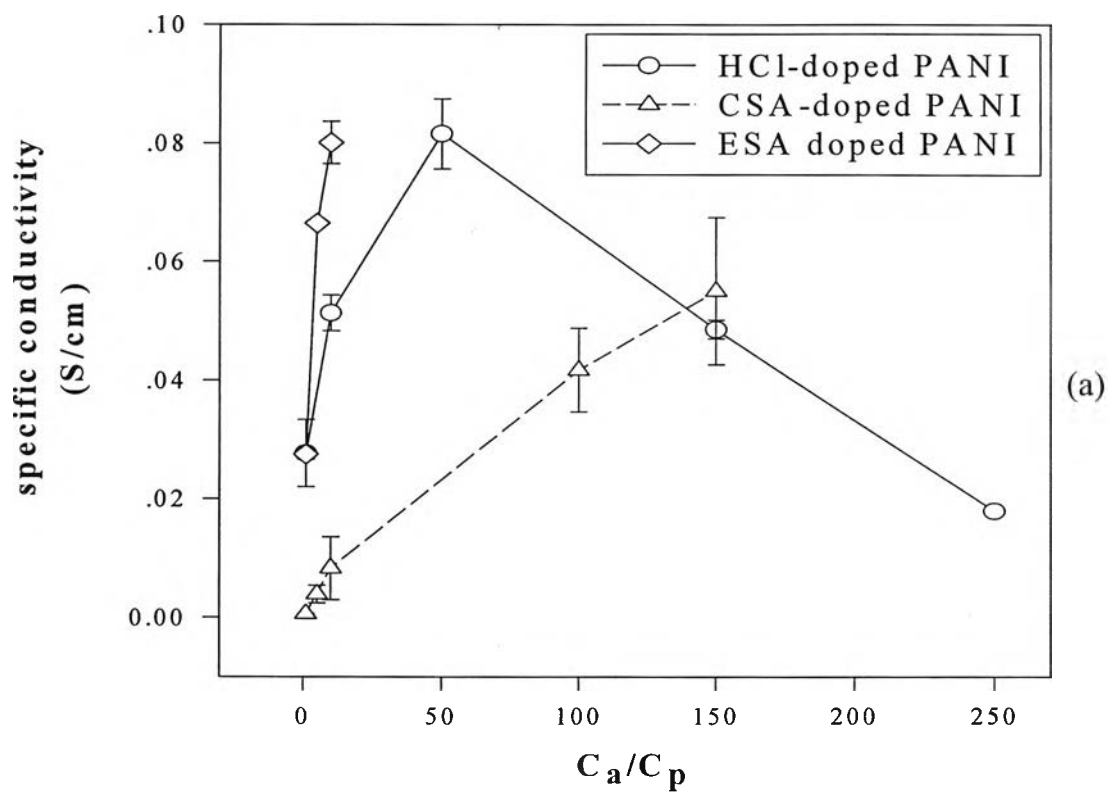
Fig. 4.21 The electrical conductivity as a function of acid concentration of the HCl and CSA doped polyaniline films: (a) C_a/C_p; and (b) N_a/N_p.
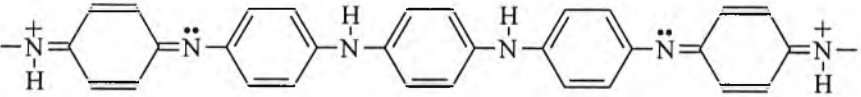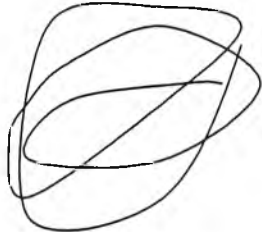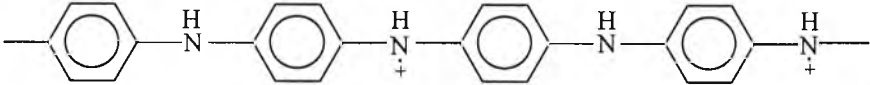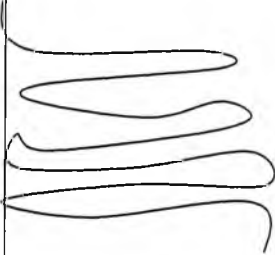
This graph shows that the electrical conductivity of the HCl doped polyaniline films sharply increases for C_a/C_p between 5 and 50. Beyond $C_a/C_p = 50$, $N_a/N_p = 496$, the electrical conductivity rapidly decreases. The maximum electrical conductivity of HCl doped polyaniline is at $C_a/C_p = 50$, $N_a/N_p = 496$ corresponding to the highest doping level. For CSA and ESA doped polyaniline films, the electrical conductivity increases linearly with doping ratio.

For the HCl doped polyaniline, at the beginning the electrical conductivity increased due to an increase in the doping level. Because the delocalization of electrons in the interchain and intrachain direction and the highest degree of crystallinity (Allcock *et al.* 1990), the maximum electrical conductivity of HCl doped polyaniline was obtained. At $C_a/C_p > 50$, the

electrical conductivity of the HCl doped polyaniline decreased corresponding to the decrease in the doping level. This was due to the delocalization of electrons and the lesser degree of crystallinity on the doped polyaniline chains. In case of the CSA and ESA doped polyaniline, the electrical conductivity increased because of the increase in the doping level and crystallinity.

The physical and chemical structures identifying the relation between the electrical conductivity and doping level are shown in Table 4.7.

Table 4.7 The proposed model for explanation the relationship between the electrical conductivity and doping level

Explanation	Chemical Structure	Physical Structure
- low doping level - some protonated at quinoid segment - low crystallinity - low electrical conductivity - low delocalization of electrons on doped polymer chains		
- high doping level - protonated at all quinoid segment sites - high crystallinity - high electrical conductivity - high delocalization of electrons on doped polymer chains		

4.2.4 Effect of SO_2

In this work, the HCl, CSA and ESA doped polyaniline films at various doping ratios were exposed to SO_2 gas in order to investigate the change in the electrical conductivity.

(a) Effect of Acid Type and Acid Concentration

The electrical conductivity of the HCl-doped polyaniline film at doping ratios equal to 1 and 50 before and after exposed to 1000 ppm SO_2/N_2 mixture are shown in Figure 4.22(a) and Figure 4.22(b), respectively.

From Figure 4.22(a) and (b), we can see that there is no difference in the electrical conductivity before and after the exposure to the SO_2 gas. This indicates that the HCl-doped polyaniline film does not response to the SO_2 gas.
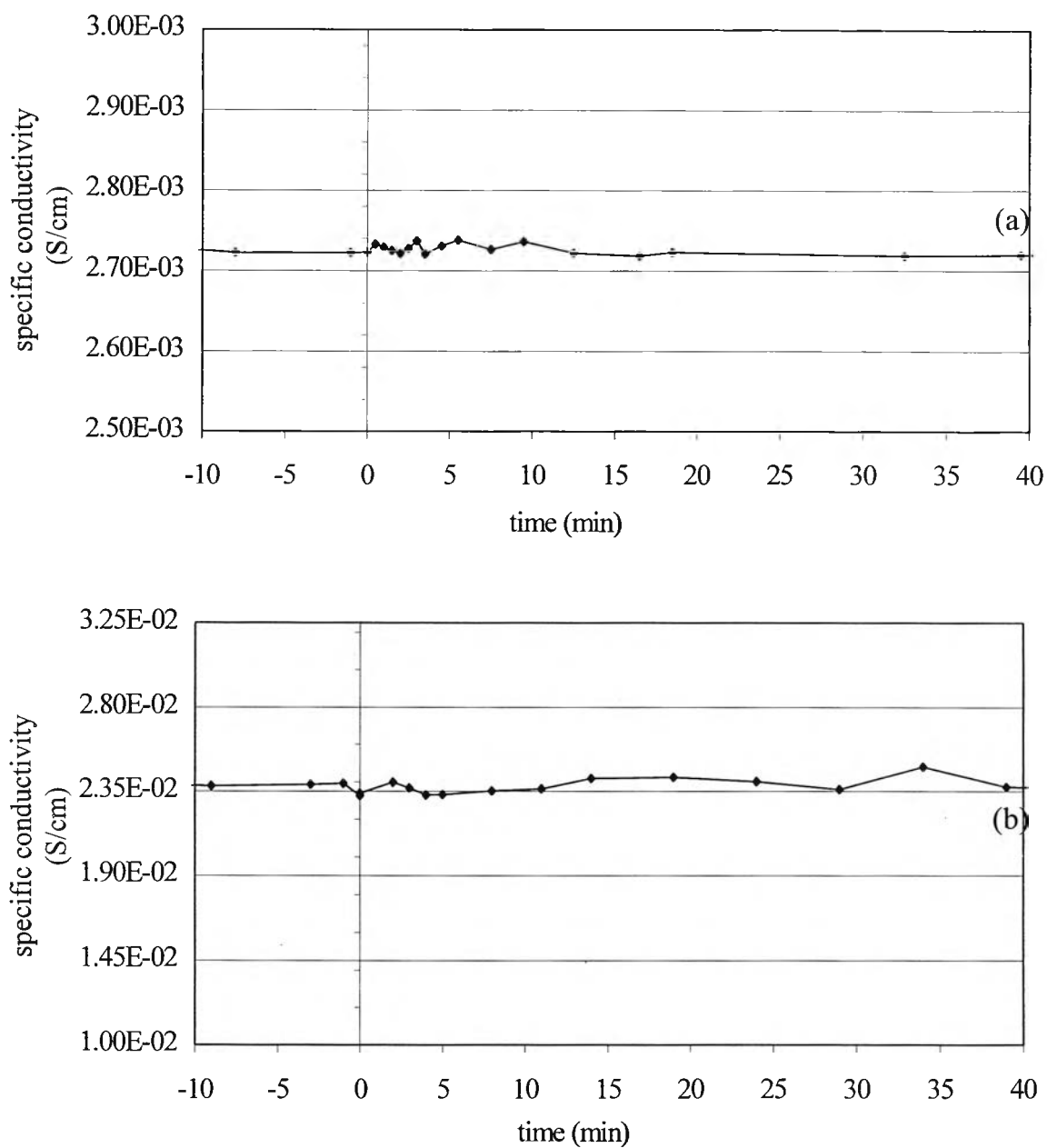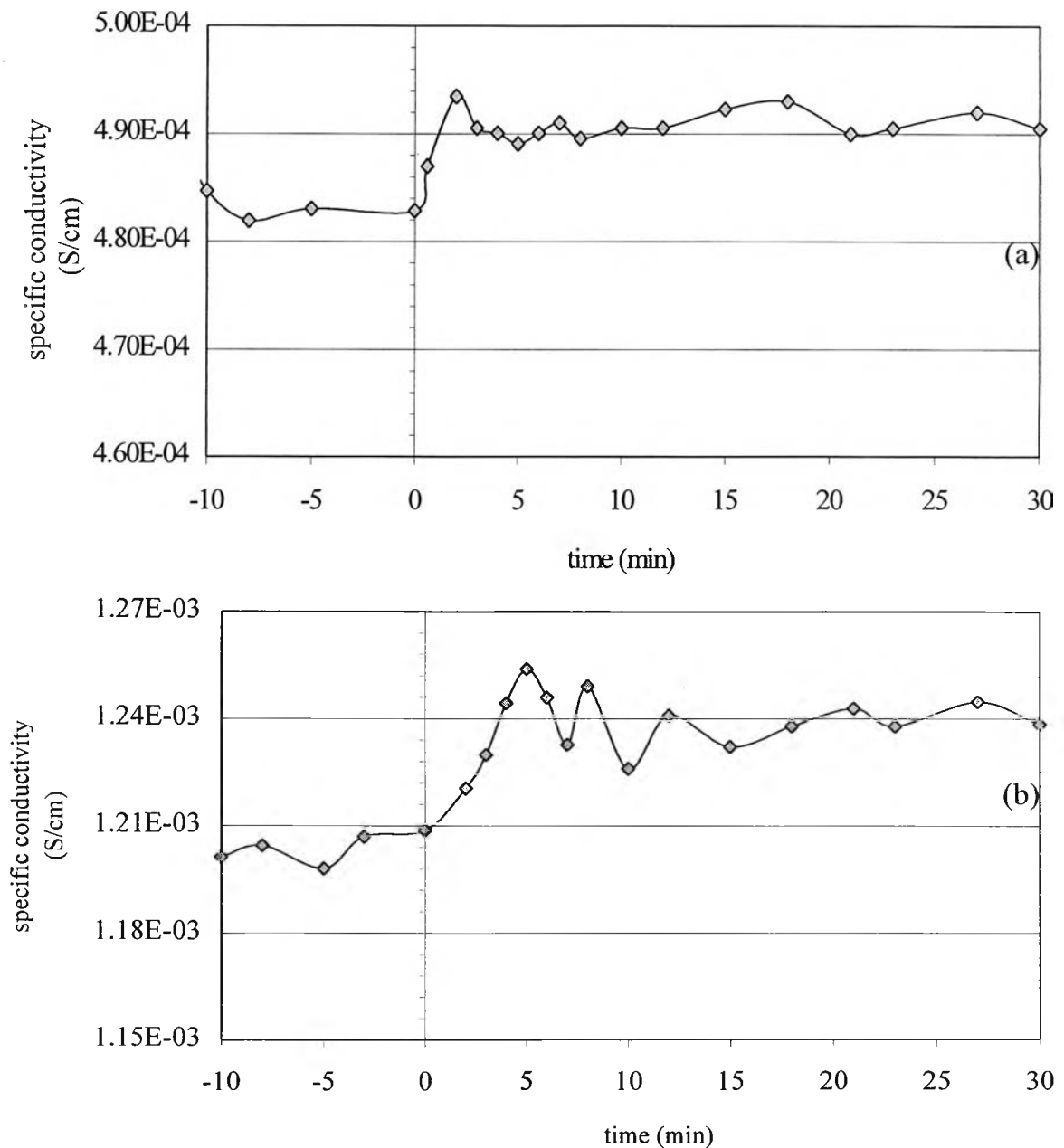
Fig. 4.22 Effect of 1000 ppm SO_2/N_2 mixture on the electrical conductivity of the HCl-doped polyaniline film at: (a) $C_a/C_p = 1$, $N_a/N_p = 9.90$; and (b) $C_a/C_p = 50$, $N_a/N_p = 496$.

The change in the electrical conductivity of CSA and ESA doped polyaniline when exposed to the SO_2 gas is shown in Figure 4.23 and Figure 4.24. In contrast to the HCl-doped polyaniline film, the response to the SO_2 gas was observed in case of the CSA and ESA doped polyaniline film.
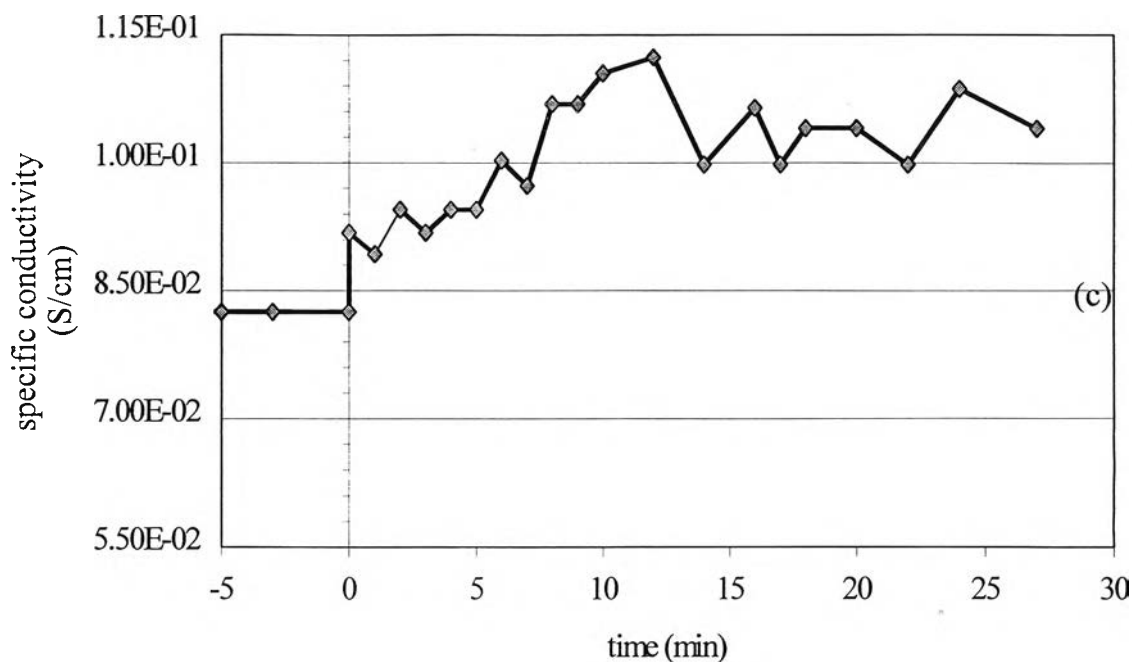
Fig. 4.23 Effect of 1000 ppm SO_2/N_2 mixture on the electrical conductivity of the CSA-doped polyaniline films at: (a) $C_a/C_p = 1$, $N_a/N_p = 1.60$; (b) $C_a/C_p = 10$, $N_a/N_p = 15.6$; and (c) $C_a/C_p = 150$, $N_a/N_p = 234$.
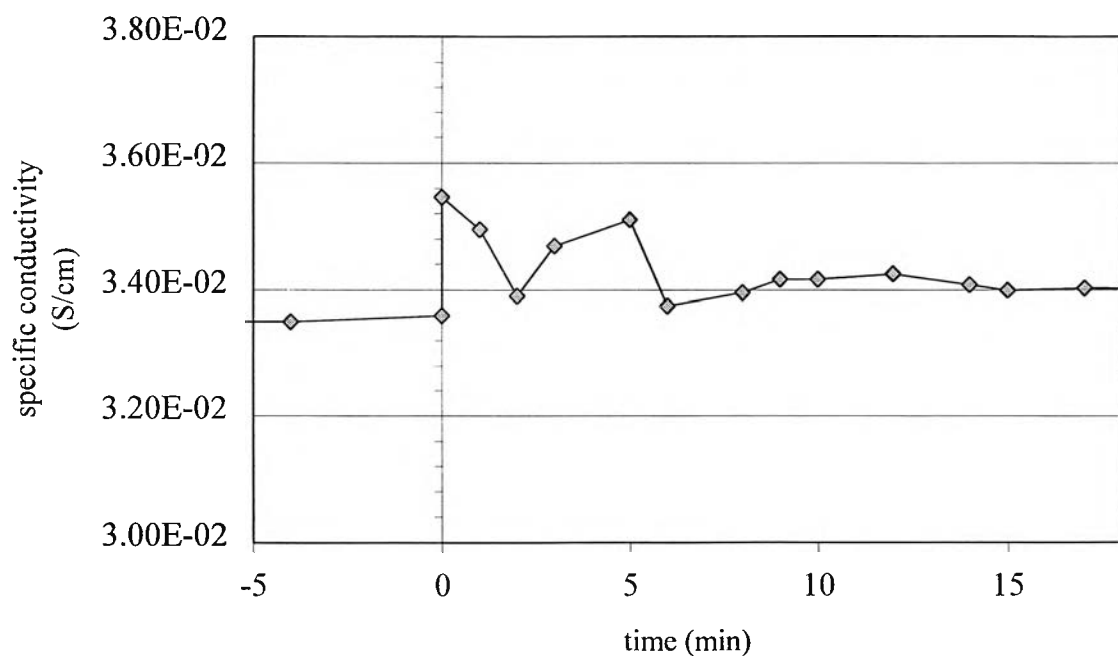

Fig. 4.24 Effect of 1000 ppm SO_2/N_2 mixture on the electrical conductivity of the ESA-doped polyaniline films at $C_a/C_p = 10$, $N_a/N_p = 32.9$.

From these figures, the increase in the electrical conductivity was observed for all doping ratios of the CSA and ESA doped polyaniline films when exposed to the 1000 ppm SO_2/N_2 mixture gas. In addition, the difference in the change in the electrical conductivity ($\Delta\sigma$) at various doping ratios and temporal response were observed. The results are listed in Table 4.8.

Table 4.8 The changes in the electrical conductivity ($\Delta\sigma$) of doped polyaniline film after exposed to 1000 ppm SO_2/N_2 mixture gas

Doped polyaniline films	C_a/C_p	N_a/N_p	$\Delta\sigma$ (S/cm)	Temporal Response (min)
CSA	1	1.60	6.34E-06	3
	10	15.6	4.84E-05	8
	150	234	3.38E-03	13
ESA	10	32.9	3.62E-03	6

The higher doping ratio the higher the changes in the electrical conductivity and temporal response occurred. The proposed models of the HCl and the CSA-doped polyanilines (functionalize acid-doped polyaniline) are shown in Figure 4.20. Because of the bulky anion group of functionalize acid (CSA and ESA), the chains of the CSA and ESA-doped polyaniline could not closely pack together in comparison with the chains of the HCl-doped polyaniline. This caused the SO_2 molecules to penetrate into the space between polyaniline chains and causes the increase the electrical conductivity. In contrast, SO_2 molecules could not penetrate into polyaniline chains of the HCl-doped polyaniline because it had a lesser spacing between polyaniline chains. Thus, the HCl-doped polyaniline did not show response to SO_2 gas. Our agreement is consistent with the XRD results as described in section 4.1.4.

The summarize of these results is shown in Figure 4.25 showing the relationship between $\Delta\sigma$ after the exposure to 1000 ppm SO_2/N_2 mixture and doping ratio of the HCl, CSA, and ESA doped polyaniline films.
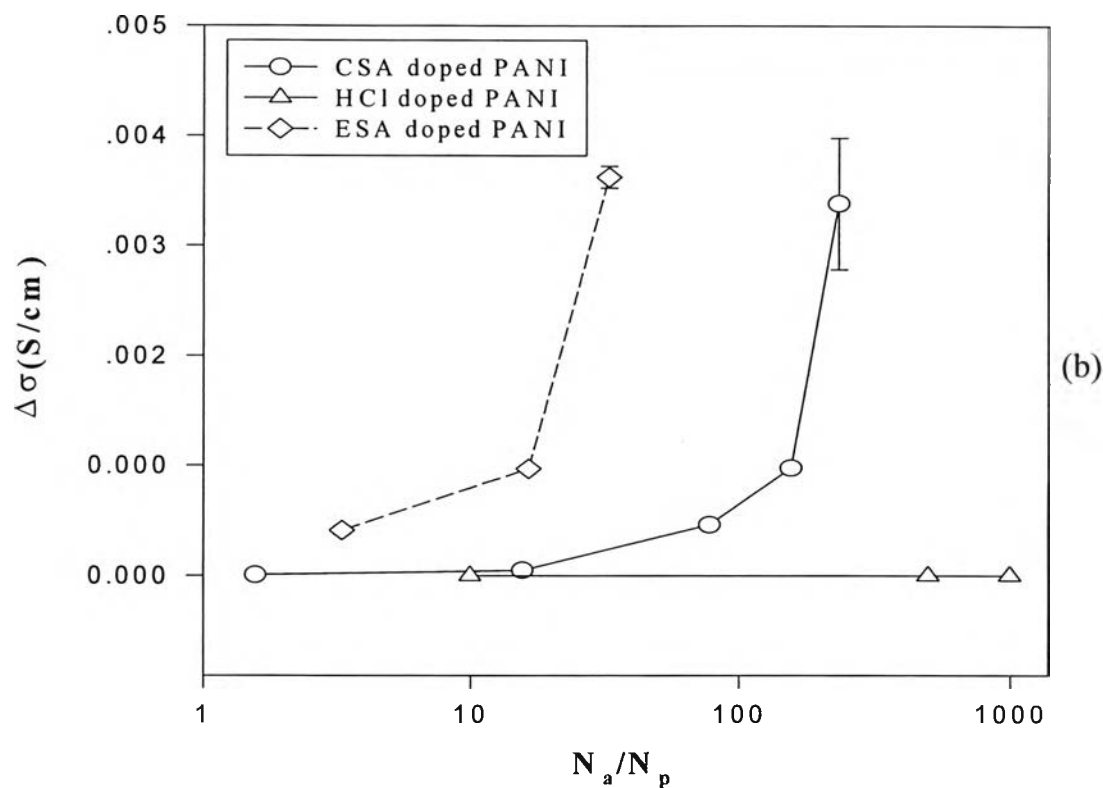

(a)
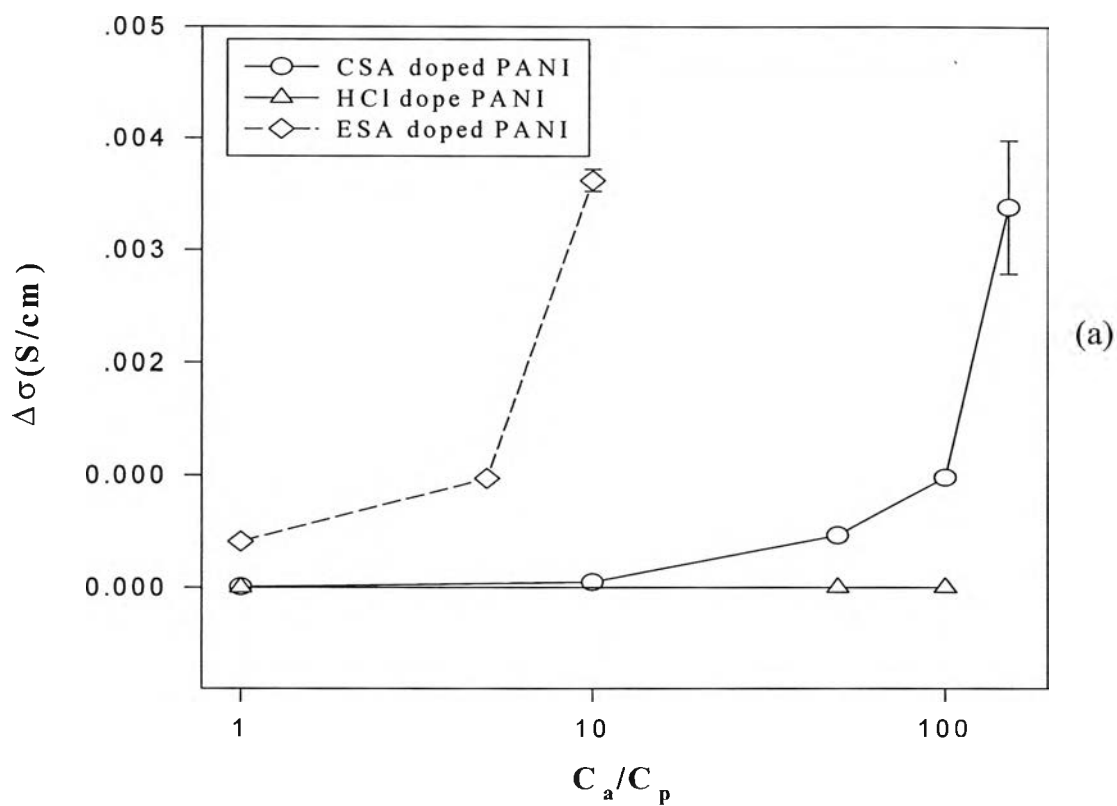
Fig. 4.25 The change ($\Delta\sigma$) in the electrical conductivity of the HCl, CSA and ESA doped polyaniline films after exposed to 1000 ppm SO_2/N_2 mixture at 25 $^{\circ}$C and 28-32 % humidity as a function of doping ratio: (a) C_a/C_p; and (b) N_a/N_p.

(b) Effect of SO_2 concentration

The relationship between percentage of change in the electrical conductivity and SO_2 concentration is shown in Figure 4.26.
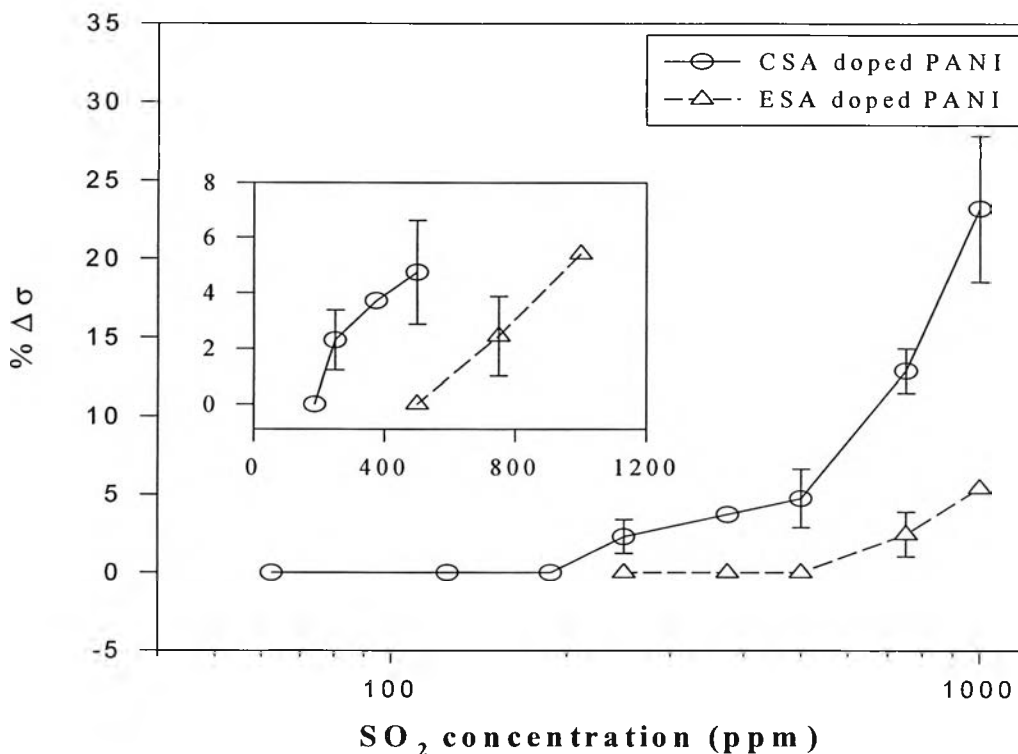

Fig. 4.26 The percentage change (% $\Delta\sigma$) in the electrical conductivity as a function of SO_2 concentration of the CSA doped polyaniline films at C_a/C_p = 150, N_a/N_p = 234: σ_0 = 8.25×10^{-2} S/cm and the ESA doped polyaniline films at C_a/C_p = 10, N_a/N_p = 32.9: σ_0 = 6.52×10^{-2} S/cm.

This graph indicates that %$\Delta\sigma$ of the CSA doped polyanilines at SO_2 concentration between 187.5 and 500 ppm increase linearly with the slope of 5.28×10^{-6} S/cm/ppm. When the SO_2 concentration is more than 500 ppm, %$\Delta\sigma$ of the CSA doped polyanilines rapidly increases linearly. For the ESA doped polyanilines, %$\Delta\sigma$ linearly increases with SO_2 concentration with the slope of 7.10×10^{-6} S/cm/ppm. The minimum SO_2 concentrations that the CSA and ESA doped polyaniline films show linear responses are 187.5 and 500 ppm, respectively.

4.2.5 Characterization of doped polyaniline after exposed to SO_2 gas

4.2.5.1 FT-IR Technique

In this work, FT-IR technique was used to investigate the difference in chemical structure of doped polyaniline after exposed to 1000 ppm SO_2/N_2 mixture gas for 45 minutes.

After doped polyaniline gas was exposed to SO_2, air purging and N_2 purging were carried on for 1 hour each, respectively. The doped polyaniline was characterized by FT-IR technique to investigate the change in chemical structure. The result of the FT-IR measurement is shown in Figure 4.27(a) and Figure 4.27(b), showing the FT-IR spectra of HCl and CSA doped polyaniline before and after the exposure to 1000 ppm SO_2/N_2 mixture. In addition, the lists of peak position and these explanations of doped polyaniline films before and after exposure to 1000 ppm SO_2/N_2 mixture gas are shown in Table 4.9.
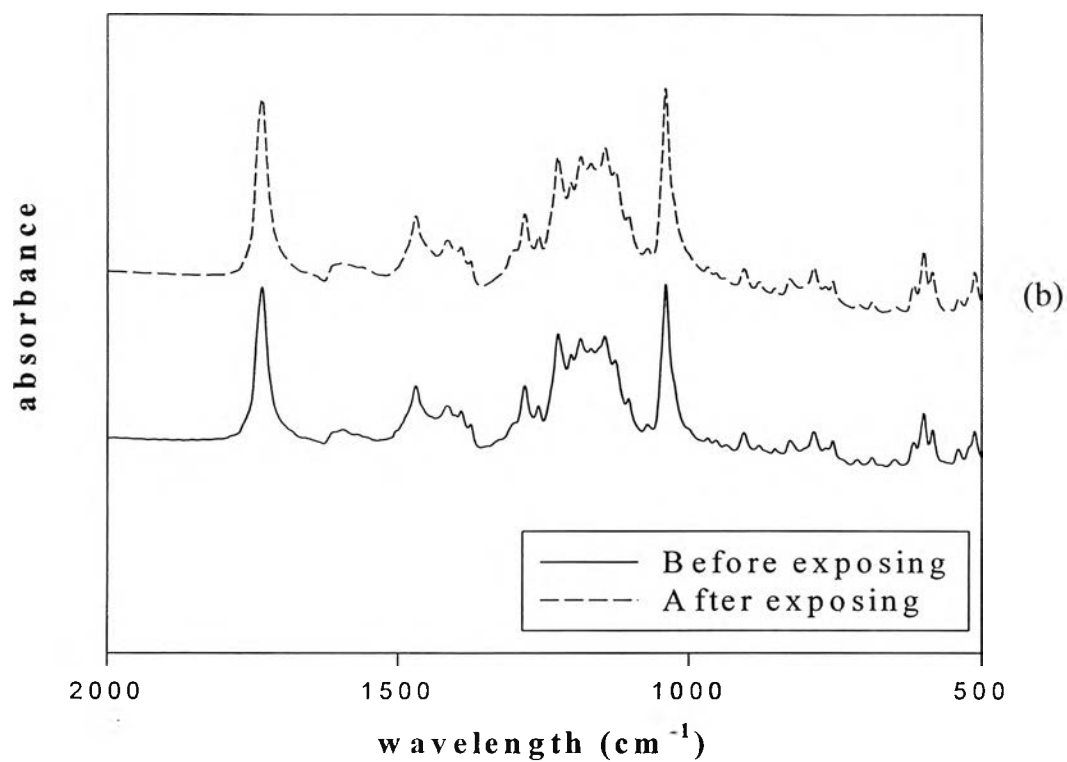

(a)
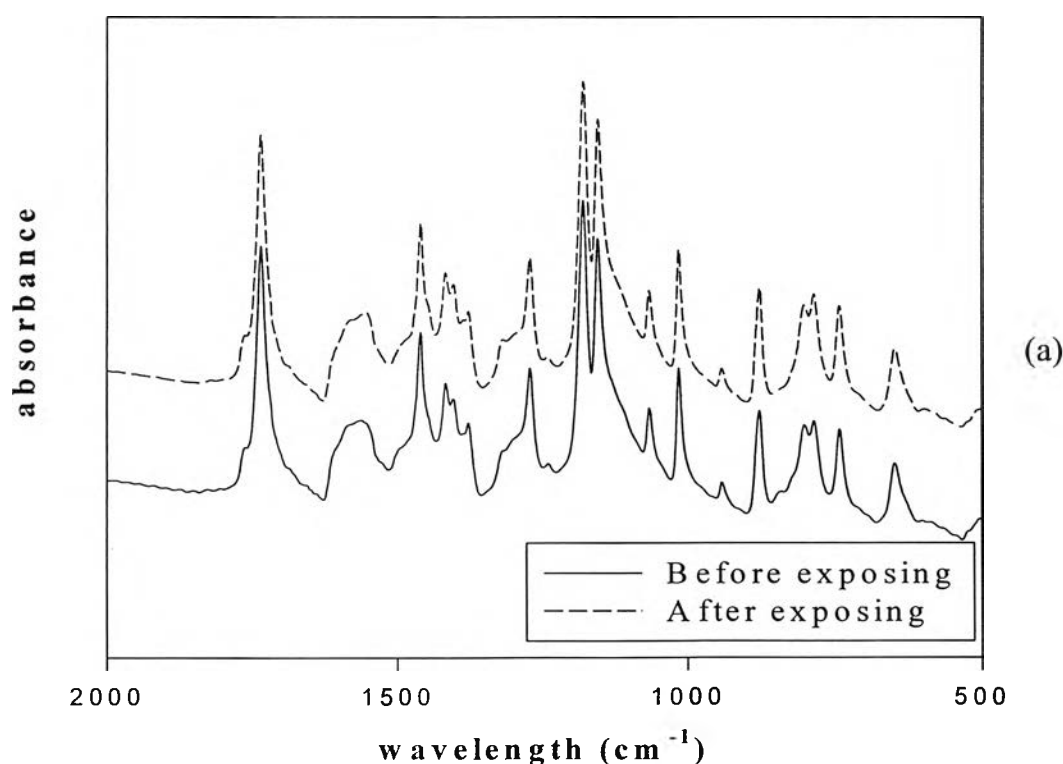
Fig. 4.27 FT-IR spectra before and after exposed to 1000 ppm SO_2/N_2 mixture of doped polyaniline: (a) the HCl-doped polyaniline at $N_a/N_p = 496$; and (b) the CSA-doped polyaniline at $N_a/N_p = 234$.

Table 4.9 The FT-IR peaks of doped polyaniline films before and after the exposure to 1000 ppm SO_2/N_2 mixture gas

Functional group	Wavelength (cm^{-1})				Ref.
	HCl at $N_a/N_p = 496$		CSA at $N_a/N_p = 234$		
	Before the exposure	After the exposure	Before the exposure	After the exposure	
C=O group of remaining NMP solvent	1735	1735	1741	1741	Milton *et al.* 1993
C=O group of camphorsulfonic acid	-	-	1741	1741	Vikki *et al.* 1996
Stretching vibration of N-bezenoid ring	1459	1458	1456	1455	Zeng *et al.* 1998
Aromatic C-N stretching vibration	1271	1271	1281	1281	Zeng *et al.* 1998
Sulfonic acid salt group	-	-	1175	1175	Chan *et al.* 1994
Aromatic in-plane blending	1154	1154	-	-	Chan *et al.* 1994

From Figure 4.27(a), Figure 4.27(b) and Table 4.9, there is no difference in the FT-IR spectra between before and after the exposure to 1000 ppm SO_2/N_2 mixture. This indicates that SO_2 molecules did not interact chemically with the doped polyaniline films. SO_2 molecules only absorbed onto the polyaniline chains and provided some interaction during the exposure. After that the desorption of SO_2 molecules occurred after purging.